Aus dem
Friedrich-Baur-Institut an der Neurologischen Klinik und Poliklinik
Klinik der Universität München
Direktor: Prof. Dr. Günter Höglinger

# TARDBP variants cause late-onset distal myopathy

Dissertation
zum Erwerb des Doktorgrades der Medizin
an der Medizinischen Fakultät
der Ludwig-Maximilians-Universität zu München

vorgelegt von
Julia Konstanze Zibold

aus
Gainesville, FL, USA

Jahr
2026

Mit Genehmigung der Medizinischen Fakultät
der Universität München

| | |
|---|---|
| Berichterstatter: | Prof. Dr. Jan Senderek |
| Mitberichterstatter: | Prof. Dr. Dr. h.c. Hubertus von Voss |
| | Prof. Dr. Julia Höfele |
| Mitbetreuung durch den promovierten Mitarbeiter: | Dr. Rolf Stucka |
| Dekan: | Prof. Dr. med. Thomas Gudermann |
| Tag der mündlichen Prüfung: | 12.02.2026 |

# Table of Contents

# List of Figures

# List of Tables

# Abbreviations

| | |
|---|---|
| °C | Degree Celcius |
| AD | Alzheimer's disease |
| ALS | Amyotrophic lateral sclerosis |
| BSA | Bovine serum albumin |
| cDNA | Complementary deoxyribonucleic acid |
| CK | Creatine kinase |
| CMV | Human cytomegalovirus |
| CT | Computed tomography |
| DAPI | 4,6-diamidino-2 phenylindole |
| DMSO | Dimethyl sulfoxide |
| DNA | Deoxyribonucleic acid |
| *E. coli* | *Escherichia coli* |
| EDTA | Ethylenediaminetetraacetic acid |
| EMG | Electromyography |
| HEK | Human embryonic kidney |
| FCS | Fetal calf serum |
| FTD | Frontotemporal dementia |
| g | Gram |
| GAPDH | Glyceraldehyde 3-phosphate dehydrogenase |
| GFP | Green fluorescent protein |
| HA | Influenza hemagglutinin |
| His6 | Hexahistidine |
| IF | Immunofluorescence |
| IPTG | Isopropyl β-D-1-thiogalactopyranoside |
| kb | Kilobase |
| kDa | Kilodalton |
| L | Liter |
| LB | Luria-Bertani |
| LCD | Low complexity domain |
| M | Molar |
| MBP | Maltose binding protein |
| MCS | Multiple cloning site |
| min | Minutes |

Abbreviations

| | |
|---|---|
| mL | Milliliter |
| mM | Millimolar |
| MTT | 3-(4,5-dimethylthiazol-2-yl)-2,5-diphenyltetrazolium bromide |
| nm | Nanometer |
| ng | Nanogram |
| NLS | Nuclear localization signal |
| NSC | Motor neuron-like cells |
| NTD | N-terminal domain |
| OD | Optical density |
| ORF | Open reading frame |
| PBS | Phosphate-buffered saline |
| PCR | Polymerase chain reaction |
| PD | Parkinson's disease |
| PMSF | Phenylmethylsulfonyl fluoride |
| rcf | Relative centrifugal force |
| rpm | Revolutions per minute |
| RRM | RNA-recognition motifs |
| RT | Room temperature |
| SDD-AGE | Semi-denaturing detergent agarose gel electrophoresis |
| SDS-PAGE | Sodium dodecyl sulfate-polyacrylamide gel electrophoresis |
| sec | Seconds |
| SEC | Size exclusion chromatography |
| SEM | Standard error of the mean |
| *TARDBP* | Transactive response DNA binding protein |
| TBS-T | Tris-buffered saline with 0.1 % Tween20 |
| TDP-43 | Transactive response DNA binding protein of 43 kDa |
| TEV | Tobacco etch virus |
| TIA1 | T-cellular antigen-1 |
| Tris | Tris-(hydroxymethyl)-aminomethane |
| WT | Wild-type |
| WB | Western blot |
| µg | Microgram |
| µL | Microliter |
| µM | Micromolar |

# 1 Introduction

## 1.1 Distal myopathy

### 1.1.1 Terminology of distal myopathies

Distal myopathies represent a genetically and clinically heterogeneous group of rare Mendelian disorders, primarily characterized by weakness of the distal musculature and a myopathic pattern on diagnostic testing. The term ‘distal myopathy’ was first coined by Gowers in 1902 in the context of early efforts to differentiate primary muscle diseases from neurogenic atrophies (1, 2). The earliest comprehensive study of familial cases of distal myopathy was published by Welander in 1951, almost half a century later, followed by the first identification of a genetic cause by Liu in 1998 (3, 4). Since then, numerous distinct pathogenic variants have been discovered in an ever-growing number of genes, reflecting substantial molecular heterogeneity (5). While distal muscle weakness can be a feature of both acquired muscle disorders and inherited myopathies, the term ‘distal myopathy’, in the stricter sense, refers to genetically determined conditions (6).

### 1.1.2 Characterization of distal myopathies

Distal myopathies are rare and occur in fewer than 1 in 100,000 individuals, according to an epidemiological study conducted in Northern England (7). Although their overall impact on society is minimal, these conditions significantly impact the daily lives of patients and their families. The classification of distal myopathies is based on the age of symptom onset, inheritance pattern, and the underlying genetic variant (8). Typically manifesting during adulthood (9), distal myopathies present with muscle weakness and wasting of the hands and feet. The initial pattern often includes anterior leg involvement, causing problems with toe-lifting and plantar flexion. Upper limb weakness commonly affects finger extensors and intrinsic hand muscles, which leads to reduced grip strength (10). Over time, additional features may emerge, including proximal muscle weakness, bulbar impairment, respiratory muscle insufficiency, and cardiac abnormalities (such as conduction disorders, arrhythmias, or cardiomyopathy) (10). The disease course is usually characterized by the slow progression of symptoms without a reduction in life expectancy. However, quality of life can be considerably affected due to the progressive limitation of mobility, potentially leading to loss of ambulation.

### 1.1.3 Diagnostic approach and treatment of distal myopathies

Patients with suspected distal myopathy should undergo a comprehensive clinical examination, with particular attention to muscle strength, signs of atrophy, and potential involvement of bulbar muscles or the cardiac and respiratory systems. Serum creatine kinase (CK) levels are highly variable, ranging from normal or near normal to markedly elevated, occasionally up to 100 times the upper limit of the reference range (2). On electromyography (EMG), motor unit potentials often exhibit reduced amplitude, brief duration, and a polyphasic pattern, findings characteristic of a myopathic lesion (10). Medical imaging (ultrasound, computed tomography (CT), magnetic resonance imaging) can be employed to delineate patterns of muscle involvement, detect subclinical muscle remodeling, and guide the selection of appropriate muscle biopsy sites (9). Histological findings in distal myopathies are variable, ranging from nonspecific myopathic changes, such as nuclei internalization and muscle fiber size variability, to more specific abnormalities like myofibrillar disarray and rimmed vacuoles (10). Further diagnostic workup includes electrocardiography and echocardiography to evaluate potential cardiac involvement, as well as pulmonary function testing to assess respiratory function (11).

Genetic testing plays a central role in identifying the underlying molecular etiology of the disease (12). To date, pathogenic variants in more than 20 genes have been associated with various forms of distal myopathy. Despite these advances in genetic diagnostics, many individuals and families with distal myopathy still lack a definitive molecular diagnosis, indicating the likely existence of additional, yet undiscovered, distal myopathy genes. Furthermore, even when a variant is identified in a known disease-associated gene, it may be classified as a variant of uncertain significance, limiting its diagnostic utility. In such cases, a muscle biopsy can provide valuable diagnostic support. The presence of a myopathic pattern, especially specific histopathological features such as rimmed vacuoles or myofibrillar disintegration, can support the diagnosis.

Treatment is limited to symptomatic management. This includes physical therapy and the use of assistive devices such as canes or wheelchairs to support mobility. Regular follow-up is recommended to monitor for potential complications, especially cardiac and pulmonary decline (12). To date, no effective disease-modifying therapies are available for distal myopathies (12). However, the emergence of gene-based therapeutic approaches in other hereditary neuromuscular disorders (13) highlights the importance of identifying the precise molecular etiology of distal myopathies, which may pave the way for targeted treatments in the future.

### 1.1.4 Differentiating myopathy from motor neuron disease

The clinical symptom of distal muscle weakness is associated with both muscle diseases and certain motor neuron diseases. Among the latter, amyotrophic lateral sclerosis (ALS) is the most prominent, with a prevalence of 5.4 per 100,000 people in European countries (14). ALS involves progressive degeneration of cortical, bulbar, and spinal motor neurons, ultimately leading to generalized paralysis and premature mortality (14). Initial manifestations often include distal muscle weakness, muscle cramps, and fasciculations, while in other patients, the disease may begin with dysphagia and dysarthria (15). The mean age at onset is 62 years, and death usually occurs within two to four years, most often due to respiratory failure (14). ALS can be associated with frontotemporal dementia (FTD), characterized by cognitive symptoms, such as apathy and aphasia (15). Given the distinct underlying pathologies, clinical manifestations, and prognoses of distal myopathies and motor neuron diseases, accurate diagnosis is essential for appropriate patient management and counselling. Several features from the clinical examination and diagnostic procedures allow for a clear distinction between myopathy and motor neuron disease (**Table 1**).

**Table 1: Comparison of distal myopathy and amyotrophic lateral sclerosis**

| | **Distal myopathy** | **Amyotrophic lateral sclerosis** |
|---|---|---|
| **Pathology** | Primary muscle disease | Motor neuron disease |
| **Course of disease** | Slow progression with usually normal life expectancy | Fatal within a median of two to four years following disease onset |
| **Manifesting symptoms** | Symmetric distal muscle weakness and atrophy | Asymmetric muscle weakness and atrophy, muscle cramps, fasciculations, dysarthria, dysphagia |
| **Other symptoms appearing over time** | Proximal muscle weakness; potential involvement of bulbar muscles, cardiac and respiratory systems | Generalized paresis, bulbar and respiratory dysfunction, cachexia, fatigue; ALS-FTD: cognitive decline, behavioral abnormalities |
| **Deep tendon reflexes** | Normal, reduced, or absent | Brisk reflexes, pyramidal tract signs |
| **Electromyography** | Myopathic pattern | Neurogenic pattern |
| **Genetic contribution** | Monogenic diseases | Usually sporadic, 5-10% familial cases |

## 1.2 Transactive response DNA-binding protein of 43 kDa (TDP-43)

### 1.2.1 Structure and function of TDP-43

The transactive response DNA binding protein of 43 kDa (TDP-43, MIM: 605078) is encoded by the *TARDBP* gene on the short arm of chromosome 1 (16). It was initially described as a transcriptional repressor of the TAR DNA element of human immunodeficiency virus type 1, from which its name is derived, and was later identified as a splicing regulator of the *CFTR* gene, which is mutated in cystic fibrosis (16, 17). TDP-43 is now recognized as a multifunctional RNA-binding protein with diverse roles in RNA metabolism, including regulation of mRNA stability, alternative splicing, and microRNA biogenesis (17-19). Structurally, human TDP-43 consists of 414 amino acids and is organized into several distinct domains: an N-terminal region that includes a nuclear localization signal (NLS), two RNA-recognition motifs (RRMs), and a C-terminal low-complexity domain (LCD), which is intrinsically disordered (17, 20) (**Figure 1**). The LCD shares sequence similarity with prion-like domains and mediates protein-protein interactions. It also promotes the formation of biomolecular condensates through phase separation, a property implicated in both physiological function and pathological aggregation of TDP-43 (21, 22).

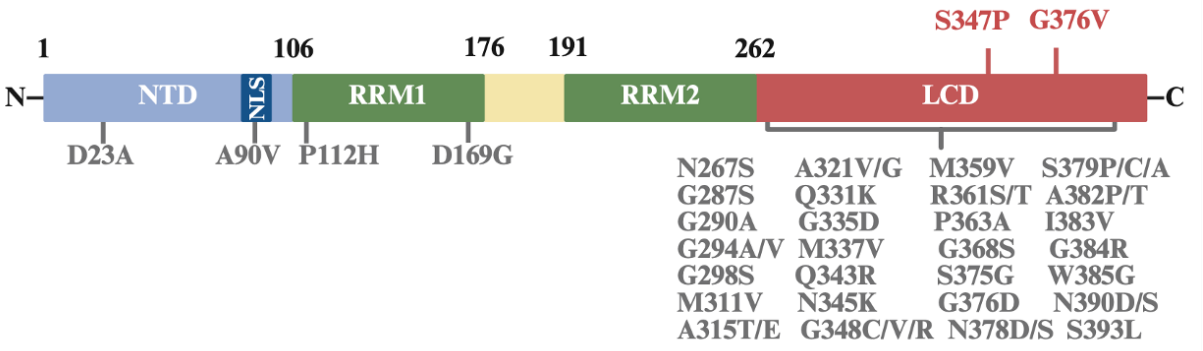


**Figure 1: TDP-43 structure and disease-causing variants**

Schematic presentation of human TDP-43 and positions of disease-associated variants. The protein consists of an N-terminal domain (NTD) with a nuclear localization sequence (NLS), two RNA-recognition motifs (RRM), and a C-terminal low complexity domain (LCD). The myopathy-associated variants are highlighted at the top (red), and a selection of ALS-associated variants is shown at the bottom (grey). The figure was adapted from (23) and created with BioRender.

### 1.2.2 TDP-43 cytoplasmic redistribution and granule formation

Under physiological conditions, TDP-43 is mainly a nuclear protein but shuttles between the nucleus and cytoplasm (24). However, under pathological conditions, TDP-43 loses its diffuse nuclear localization and instead accumulates in cytoplasmic granules (25, 26). The precise

mechanisms driving this subcellular redistribution and granule formation are not fully understood and remain intensively debated. Altered subcellular localization has been attributed to disruptions of nucleocytoplasmic transport, presumably triggered by factors such as cellular stress, posttranslational modifications, or *TARDBP* gene variants (see section 1.2.3) (23). The formation of TDP-43 granules has been suggested to involve phase separation, a process that allows proteins like TDP-43 to demix from a homogeneous solution to form liquid-like condensates through multivalent intermolecular interactions (27). Phase separation serves as a physiological mechanism for generating dynamic and reversible biomolecular assemblies, facilitating efficient resource allocation and supporting cellular homeostasis, particularly under stress conditions (28). However, when the regulatory mechanisms of phase separation are disrupted, such as by chronic cellular stress, *TARDBP* variants, changes in subcellular localization, or impaired RNA and protein interactions, these condensates can undergo aberrant phase transitions, ultimately resulting in the formation of high-molecular-weight assemblies and the pathological conversion from soluble protein to stable, insoluble aggregates (29, 30).

### 1.2.3 Involvement of TDP-43 in disease

Cytoplasmic TDP-43-positive granules were first observed in neurons and glial cells from ALS and FTD brains, where they were found to undergo posttranslational modifications such as ubiquitination, phosphorylation, and intramolecular cleavage (31, 32). Since then, cytoplasmic TDP-43 inclusions have also been detected in the central nervous system of patients with other neurodegenerative disorders, including Alzheimer's disease (AD), dementia with Lewy bodies, Parkinson's disease (PD), and Huntington's disease (33-37). Collectively, conditions featuring TDP-43 aggregates are now often referred to as TDP-43 proteinopathies (38, 39), underscoring the protein's pathological role across a broad disease spectrum.

The pathophysiological significance of TDP-43 dysfunction was further underscored when *TARDBP* variants were detected in several ALS cases (40-42). These findings indicated that abnormal TDP-43 function and TDP-43 granules can directly contribute to neuronal damage, rather than being a secondary consequence of neurodegeneration. Subsequently, *TARDBP* variants were also detected in individuals affected by FTD, AD, and PD (43-45). Around 3% of familial ALS cases and 1.5% of sporadic cases can be attributed to *TARDBP* variants (46), with most variants clustering in the LCD of TDP-43 (47). Functional studies of these disease-causing variants have revealed several pathogenic features, including an increased propensity for the formation of cytoplasmic TDP-43 granules, loss of nuclear localization, altered responses to cellular stress, and changes in phase separation dynamics (30, 48-52). However,

the results of these studies have been notably variable, even for the same variant, indicating that the impact of individual variants may be influenced by experimental context or cellular environment. Furthermore, while some variants clearly enhance cellular toxicity (53, 54), others appear to have neutral or context-dependent effects (49, 55).

### 1.2.4 Role of TDP-43 in skeletal muscle pathology

Notably, TDP-43 pathology is not restricted to the nervous system. TDP-43-positive granules have also been discovered in the cytoplasm of skeletal muscle fibers of patients affected by rimmed vacuole myopathies (such as sporadic inclusion body myositis and inclusion body myopathy with Paget's disease of bone and FTD) as well as myofibrillar myopathies (56-60). These aggregates were frequently accompanied by a reduction or complete loss of TDP-43 localization in the myonuclei (57, 58, 60).

In contrast to the situation in the nervous system, where *TARDBP* variants have been implicated in familial ALS, no primary muscle disease was known to be caused by *TARDBP* variants until recently. However, the presence of TDP-43-positive granules in muscle tissue led to the hypothesis that *TARDBP* variants could directly contribute to skeletal muscle disorders, analogous to their role in neurodegenerative diseases. Building on this hypothesis, patients with etiologically unexplained myopathies were screened for *TARDBP* variants at LMU University Hospital, LMU Munich, and the Faculté de Médecine Rockefeller, Université Claude Bernard Lyon. This screening identified two *TARDBP* missense variants, as further detailed in section 1.3. Moreover, while this thesis was being finalized, a *TARDBP* frameshift variant, p.Trp385IlefsTer10 (W385I-fs), was reported in cases of rimmed vacuole myopathy (61).

## 1.3 Identification of myopathy-associated *TARDBP* variants

Genome-wide linkage analysis, exome-sequencing, and segregation studies by Sanger sequencing identified the *TARDBP* variant p.Gly376Val (G376V) in two reportedly unrelated French families affected by late-onset, autosomal-dominant distal myopathy. Additionally, in an isolated German patient with distal myopathy, a second *TARDBP* variant, p.Ser347Pro (S347P), was detected (**Figure 2A**). Both variants affect amino acid residues that are strictly conserved during the evolution of TDP-43 (**Figure 2B** and **Table 20** in the appendix). Computational pathogenicity prediction tools classified both variants as deleterious (**Table 21** in the appendix). Furthermore, neither variant was found in public databases covering human genomic variation (**Table 22** in the appendix).

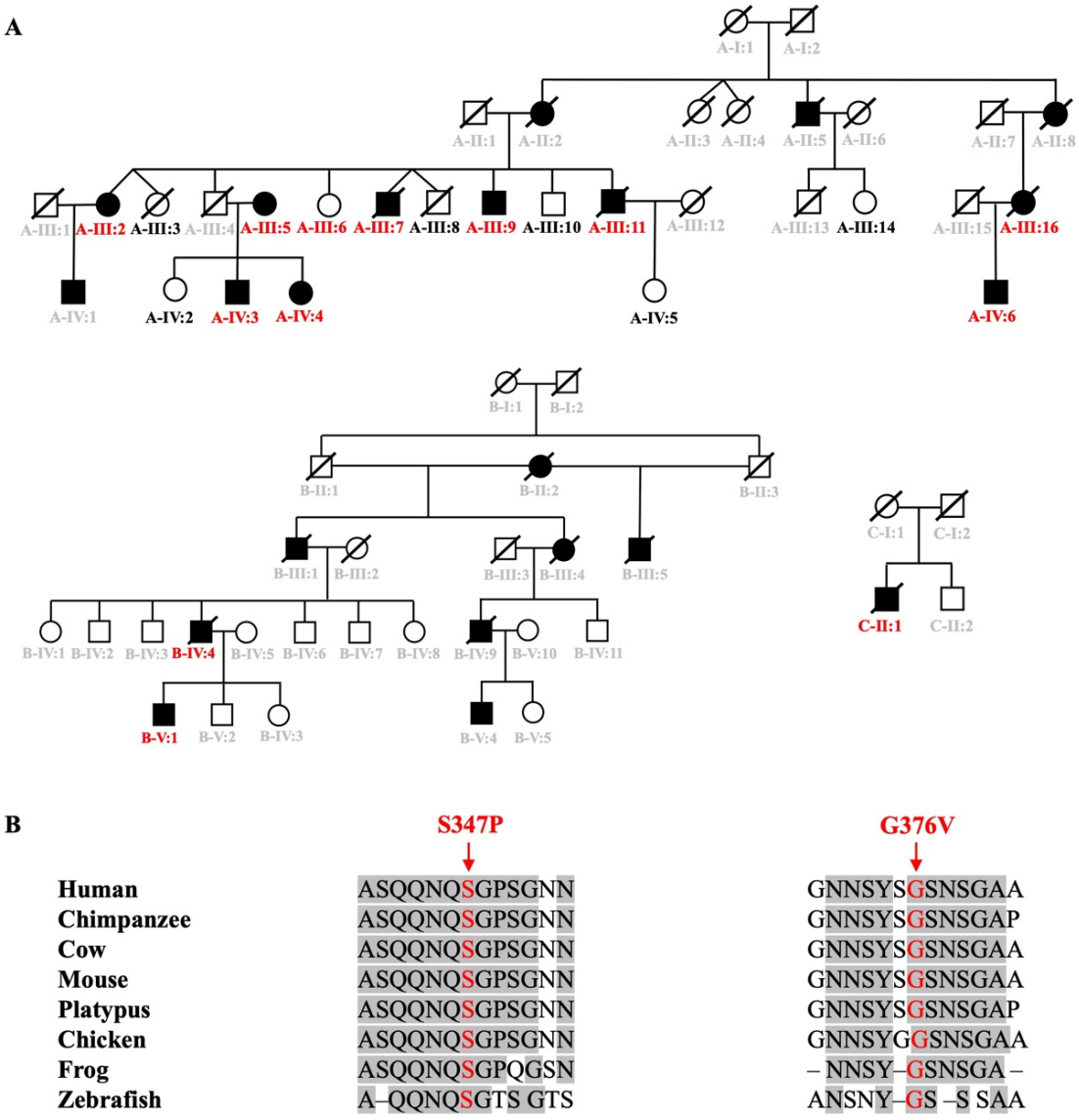


**Figure 2: Identification of *TARDBP* variants in distal myopathy families** (adapted from (62))

**A) Pedigrees of the families with *TARDBP* variants**

Two *TARDBP* variants were identified in three families. The variant p.Gly376Val was detected in families A and B, while p.Ser347Pro was found in the DNA of the index patient of family C. Filled symbols represent affected individuals, whereas empty symbols indicate individuals without a diagnosis of distal myopathy. Circles denote females, squares denote males, and deceased individuals are marked with a diagonal line. Individuals labeled in black tested negative for *TARDBP* variants, those labeled in red carry the familial *TARDBP* variant, and individuals with grey labels were not tested due to the unavailability of DNA samples.

**B) Multiple sequence alignments of TDP-43 from several species**

The variants identified in *TARDBP* alter residues that show strong evolutionary conservation. Arrows indicate the positions of missense variants observed in patients. Residues highlighted with a grey background represent conserved amino acids. Human (*H. sapiens*): Q13148, chimpanzee (*P. troglodytes*): XP_016809429, cow (*B. taurus*): G3MX91, mouse (*M. musculus*): Q921F2, platypus (*O. anatinus*): ENSOANT00000021034, chicken (*G. gallus*): Q5ZLN5, frog (*X. tropicalis*): Q28F51, and zebrafish (*D. rerio*): NP_958884.

All affected individuals showed distal muscle weakness and atrophy, which initially started in the lower extremities, the upper limbs, or both simultaneously (**Figure 3A, B**, and **Table 2**). Clinical symptoms developed at a median age of 50 years and progressed over time, leading to loss of independent ambulation in some patients. Additional features observed in certain individuals included pulmonary dysfunction and cardiac disease. No signs of pyramidal tract dysfunction, cognitive impairment, or behavioral abnormalities were observed.

**Table 2: Clinical presentation of *TARDBP*-related distal myopathy** (adapted from (62))

| **Individual** | **A: III-5** | **A: III-7** | **A: III-9** | **A: III-11** | **A: III-16** | **A: IV-3** | **A: IV-6** | **B: IV-4** | **B: V-1** | **C: II-1** |
|---|---|---|---|---|---|---|---|---|---|---|
| **Sex** | F | M | M | M | F | M | M | M | M | M |
| **Onset age (y)** | 45 | 54 | 50 | 50 | 69 | 50 | 49 | 40 | 40 | 63 |
| **First symptoms** | distal UL | distal UL & LL | distal UL | distal UL & LL | distal UL & LL | distal UL | distal LL | UL | distal LL | distal LL |
| **Asymmetric involvement** | Yes | No | Yes | Yes | No | Yes | Yes | No | Yes | No |
| **Impaired ambulation**[a)] | + | + | ++ | +++ | + | + | + | ++ | ++ | ++ |
| **Dysphagia** | Yes | Yes | Yes | Yes | Yes | Yes | No | Yes | No | No |
| **Exertional dyspnea** | Yes | Yes | Yes | Yes | Yes | Yes | Yes | Yes | No | No |
| **Cardiac disease** | No | No | No | Yes[b)] | Yes[c)] | No | Yes[d)] | No | Yes[e)] | No |
| **CK level (IU/L)** | 157 | N | N | 500 | 173 | NP | 500 | N | 430 | 370 |
| **Myogenic EMG** | Yes | NP | Yes | Yes | Yes | NP | Yes | Yes | Yes | Yes |

Abbreviations: CK = creatine kinase; EMG = electromyography; F = female; LL = lower limbs; M = male; N = within normal limits; NP = not performed; UL = upper limbs; y = years

[a)] Degree of impaired ambulation at most recent visit: + = difficulties to walk, ++ = ambulation with support, +++ = wheelchair-bound; [b)] hypertrophic cardiomyopathy; [c)] atrial fibrillation; [d)] left bundle branch block; [e)] one episode of ventricular tachycardia

Levels of serum CK were normal or mildly elevated. EMG findings were consistent with a myopathic process, whereas nerve conduction studies were normal. CT imaging demonstrated atrophy of distal limb musculature (**Figure 3C**). Light microscopy of muscle biopsies showed chronic myopathic changes, including endomysial fibrosis, fiber atrophy, centralized nuclei,

and sarcoplasmic vacuoles (**Figure 3D**). Immunohistochemistry for phosphorylated TDP-43 revealed sarcoplasmic granules associated with vacuolar structures (**Figure 3E**).

One individual (A-III:6), reported as clinically unaffected, was found to carry the *TARDBP* variant. This is most likely attributable to incomplete penetrance of the variant or underreporting of symptoms, as this individual had not undergone assessment at a specialized neuromuscular center.

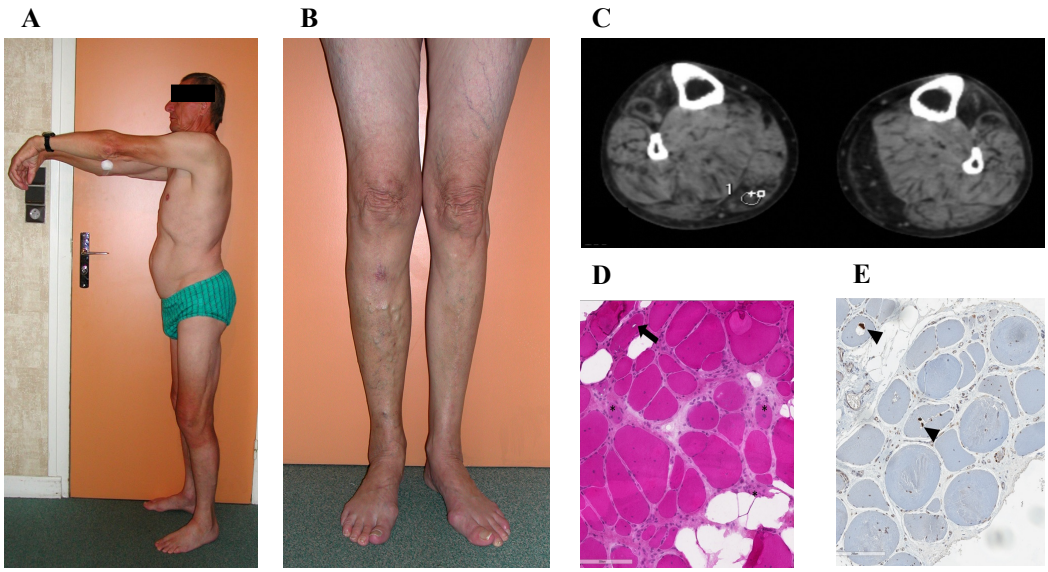


**Figure 3: Clinical and histopathological features of *TARDBP*-related distal myopathy** (adapted from (62))

**A) Clinical photograph of individual A-III:11 (age 67)**
The patient exhibited symmetric upper limb extensor muscle weakness.
**B) Clinical photograph of individual A-III:5 (age 70)**
The patient presented with muscle atrophy in the anterior compartment of the left distal leg.
**C) Skeletal muscle CT scan of subject A-IV:6 (age 51)**
Imaging revealed thigh muscle atrophy.
**D) Muscle biopsy from individual B-IV:4 (age 73)**
Hematoxylin-phloxine-saffron (HPS) staining revealed rimmed vacuoles (arrow), myofiber atrophy and necrosis (asterisks), centralized nuclei, and fatty infiltration. Scale bar: 200 µm.
**E) Muscle biopsy from individual B-IV:4 (age 73)**
Immunostaining for phosphorylated TDP-43 showed granular deposits in the cytoplasm (arrowheads). Scale bar: 200 µm.

# 2 Aims of the Study

Following the recent identification of *TARDBP* variants in patients with distal myopathy, this study was designed to explore the molecular and cellular pathways through which these variants cause the disease. Specifically, the work focused on the functional characterization of newly identified myopathy-associated *TARDBP* variants, evaluating whether they recapitulate known key features of TDP-43 pathology, particularly its aggregation-like behavior, and how their effects may differ from those of wild-type TDP-43 and ALS-associated variants.

To address these questions, a series of functional assays was conducted to assess whether the myopathy-associated *TARDBP* variants (i) alter the solubility of TDP-43, (ii) modify its subcellular distribution, (iii) affect its phase separation properties, (iv) change the morphology of TDP-43 condensates, and (v) influence the kinetics of detergent-resistant aggregate formation. To ensure consistency with prior studies, protocols established for wild-type and ALS-variant TDP-43 were followed, including the use of the motor neuron-like NSC-34 cell line. In addition, one of the most extensively studied ALS-associated *TARDBP* variants, p.Ala315Thr (A315T), was included as a comparator.

The findings from this work are expected to advance the understanding of the mechanisms underlying *TARDBP*-induced distal myopathy and provide a foundation for future research aimed at developing targeted therapeutic approaches.

# 3 Material and Methods

Recombinant plasmids were generated by Dr. Rolf Stucka from our research group at the Friedrich-Baur-Institute. I performed protein purification and phase separation assays at the LMU Biomedical Center (BMC) in the former laboratory of Prof. Dorothee Dormann (now at Johannes Gutenberg University Mainz), under the supervision of Dr. Lara Aletta Gruijs da Silva, with additional support from Francesca Simonetti (PhD student). All other experimental work described in this study was carried out by me in the laboratory of the Friedrich-Baur-Institute. Unless otherwise specified, procedures were performed with minor modifications to published protocols (63-65) or according to the manufacturer's instructions.

## 3.1 Laboratory equipment and reagents

**Table 3: Laboratory equipment**

| Description | Supplier |
|---|---|
| Axio Observer.Z1 field fluorescence microscope | Zeiss (Oberkochen, Germany) |
| Bandelin Sonoplus Sonicator HD 2070 | Bandelin electronics (Berlin, Germany) |
| BioShake iQ | Analytik (Jena, Germany) |
| BioTek Powerwave HT plate reader | Agilent (Santa Clara, USA) |
| Centrifuge 5417 | Eppendorf (Hamburg, Germany) |
| Freezer -20 °C, -80 °C | Heraeus (Hanau, Germany) |
| Heating block | Liebisch (Bielefeld, Germany) |
| HI 9321 Microprocessor pH Meter | Hanna Instruments (Vöhringen, Germany) |
| Incubator 37 °C | Heraeus (Hanau, Germany) |
| Mastercycler personal | Eppendorf (Hamburg, Germany) |
| Mini-PROTEAN Tetra Cell Proteingel chamber | Bio-Rad (Hercules, USA) |
| MiniSpin | Eppendorf (Hamburg, Germany) |
| Nanodrop ND-1000 Spectrophotometer | Peqlab (Erlangen, Germany) |
| Odyssey Fc Imaging System | Li-Cor Biosciences (Lincoln, USA) |
| Olympus BX61 confocal microscope | Olympus (Tokio, Japan) |
| Pipet-Aid XP | Drummond Scientific (Broomall, USA |
| Pipet tip Safe Seal SurPhob | Biozym (Hessisch Oldendorf, Germany) |
| Power Pac HC | Bio-Rad (Hercules, USA) |
| Scale Kern PRS 620-3 | Kern & Sohn (Balingen, Germany) |
| TC20 Automated Cell Counter | Bio-Rad (Hercules, USA) |
| Tecan infinite M200PRO plate reader | Tecan Group (Maennedorf, Swiss) |
| µ-Slide 18 Well - Flat chambers | Ibidi (Gräfelfing, Germany) |
| Vortex Genie 2 | Scientific Industries (New York, USA) |

**Table 4: Molecular biology kits**

| Description | Supplier |
|---|---|
| GFP-Trap Magnetic Agarose | ChromoTek (Planegg, Germany) |
| jetPEI Transfection Reagent | Polyplus (Illkirch, France) |
| Lipofectamine 2000 Transfection Reagent | Invitrogen, Thermo Fisher (Waltham, USA) |
| NucleoBond PC 500 Plasmid DNA Purification | Macherey-Nagel (Düren, Germany) |
| NucleoSpin Gel and PCR Clean-up Kit | Macherey-Nagel (Düren, Germany) |
| QuikChange Site-Directed Mutagenesis Kit | Agilent (San Diego, USA) |

**Table 5: Chemicals**

| Description | Supplier |
|---|---|
| Albumin Fraktion V | Carl Roth (Karlsruhe, Germany) |
| Bovine serum albumin (BSA) | Sigma-Aldrich (Taufkirchen, Germany) |
| Dimethyl sulphoxide | Carl Roth (Karlsruhe, Germany) |
| Dulbecco's Modified Eagle Medium (DMEM) | Gibco, Thermo Fisher (Waltham, USA) |
| Dulbecco's Phosphate Buffered Saline (PBS) | Sigma-Aldrich (Taufkirchen, Germany) |
| Ethanol 96% | Carl Roth (Karlsruhe, Germany) |
| Ethylenediaminetetraacetic acid (EDTA) | Sigma-Aldrich (Taufkirchen, Germany) |
| Fetal calf serum (FCS) | Sigma-Aldrich (Taufkirchen, Germany) |
| Fluorescence Mounting Medium | Dako, Agilent (Santa Clara, USA) |
| GlutaMax Supplement | Gibco, Thermo Fisher (Waltham, USA) |
| Hydrochloric acid fuming 37% | Carl Roth (Karlsruhe, Germany) |
| Isopropanol | Carl Roth (Karlsruhe, Germany) |
| Methanol | Carl Roth (Karlsruhe, Germany) |
| Milk powder | Carl Roth (Karlsruhe, Germany) |
| NP-40 | Sigma-Aldrich (Taufkirchen, Germany) |
| PageRuler Prestained Protein Ladder | Thermo Fisher (Waltham, USA) |
| Penicillin-streptomycin (P/S) | Sigma-Aldrich (Taufkirchen, Germany) |
| Phenylmethylsulfonyl fluoride (PMSF) | Sigma-Aldrich (Taufkirchen, Germany) |
| Phosphate buffered saline (PBS) | Sigma-Aldrich (Taufkirchen, Germany) |
| Protease Inhibitor Cocktail Tablets | Roche (Basel, Switzerland) |
| Sodium chloride (NaCl) | Sigma-Aldrich (Taufkirchen, Germany) |
| Sodium dioxoarsenite | Sigma-Aldrich (Taufkirchen, Germany) |
| Sodium deoxycholate | Sigma-Aldrich (Taufkirchen, Germany) |
| Sodium fluoride (NaF) | Sigma-Aldrich (Taufkirchen, Germany) |
| Sodium orthovanadate ($Na_3VO_4$) | Sigma-Aldrich (Taufkirchen, Germany) |
| Tetramethylethylendiamine (TEMED) | Sigma-Aldrich (Taufkirchen, Germany) |
| Trishydroxymethylaminomethan (Tris) | Carl Roth (Karlsruhe, Germany) |
| Trypsin-EDTA 0.05% | Gibco, Thermo Fisher (Waltham, USA) |
| Tween 20 | Sigma-Aldrich (Taufkirchen, Germany) |

**Table 6: Enzymes**

| Description | Supplier |
|---|---|
| AccuPrime Pfx DNA Polymerase | Invitrogen, Thermo Fisher (Waltham, USA) |
| DreamTaq Hot Start Green PCR Master Mix | Thermo Fisher (Waltham, USA) |
| Restriction endonucleases | New England BioLabs (Ipswich, USA) |
| T4 DNA Ligase | New England BioLabs (Ipswich, USA) |
| TEV protease (His6-tagged) | Prof. Dorothee Dormann |

**Table 7: Buffers and gels**

| Description | Composition/supplier |
|---|---|
| Cell lysis | |
| Cell lysis buffer | 1% SDS, 10 mM Tris-HCl pH 7.4, protease and phosphatase inhibitors |
| RIPA buffer | 150 mM NaCl, 50 mM Tris-HCl pH 8.0, 0.1% SDS, 1% NP-40, 1% sodium deoxycholate, 50 mM NaF, 1 mM $Na_3VO_4$, 200 mM PMSF, protease inhibitor cocktail |
| SDS-PAGE and western blot | |
| Running buffer | 25 mM Tris, 192 mM glycine, 0.1% SDS, pH 8.3 |
| 4-15% Mini-PROTEAN precast gels | Bio-Rad (Hercules, USA) |
| Trans-Blot Turbo 5x Transfer Buffer | Bio-Rad (Hercules, USA) |
| Blocking buffer | 5% nonfat milk in Tris-buffered saline with 0.1%, Tween20 (TBS-T) or 3% BSA in PBS |
| Co-immunoprecipitation (Co-IP) | |
| Co-IP lysis buffer | 10 mM Tris-HCl pH 7.5, 150 mM NaCl, 0.5 mM EDTA, 0.5% NP-40 |
| Co-IP wash buffer | 10 mM Tris-HCl pH 7.5, 150 mM NaCl, 0.5 mM EDTA |
| Protein purification | |
| Protein purification lysis buffer | 20 mM Tris pH 8.0, 1 M NaCl, 10 mM imidazole, 10% glycerol, 4 mM Beta-mercaptoethanol, 1 µg/mL aprotinin, 1 µg/mL pepstatin, 1 µg/mL leupeptin, $H_2O$ ad 250 mL |
| Protein purification SEC buffer | 20 mM Tris pH 8.0, 300 mM NaCl, 10% glycerol, 2mM TCEP, $H_2O$ ad 500 mL |
| Phase separation assays | |
| Phase separation phosphate buffer | 20 mM Na2HPO4/NaH2PO4 pH 7.5, 2.5% glycerol, 1 mM dithiothreitol (DTT), 150 mM NaCl, $H_2O$ ad 1 mL |

**Table 8: Primers for *TARDBP* cloning and mutagenesis**

| Oligonucleotide primer | Sequence (5'-3') |
|---|---|
| pCMV_HA_TDP43_XhoI | ATACTGCTCGAGCTATGTCTGAATATATTCGGGT |
| pCMV_HA_TDP43_NotI | CTGATAGCGGCCGCCTGCTACATTCCCCAGCCAGAAGAC |
| pEGFP_N1_TDP43_HindIII | CTGATAAAGCTTCTGCATTCCCCAGCCAGAAGACT |
| pEGFP_N1_TDP43_XhoI | ATACTGCTCGAGCTGATGTCTGAATATATTCGGGT |

(table continued on next page)

(table continued from previous page)

| Oligonucleotide primer | Sequence (5'-3') |
|---|---|
| TDP43_A315T_F | TGGTGGGATGAACTTTGGTACGTTCAGCATTAATCC |
| TDP43_A315T_R | GGATTAATGCTGAACGTACCAAAGTTCATCCCACCA |
| TDP43_G376V_F | CTGGAAATAACTCTTATAGTGTCTCTAATTCTGGTGC |
| TDP43_G376V_R | ATTGCTGCACCAGAATTAGAGACACTATAAGAGTTAT |
| TDP43_S347P_F | CCAGCAGAACCAGCCAGGCCCATCGGG |
| TDP43_S347P_R | CCCGATGGGCCTGGCTGGTTCTGCTGG |

**Table 9: Plasmids and constructs**

| Plasmids | Characteristics | Supplier |
|---|---|---|
| pCMV-SPORT6/TDP43 | CMV promoter, *TARDBP* ORF, ampicillin resistance gene (clone 5498250 (MGC:87845)) | Horizon Discovery (Cambridge, UK) |
| pCMV-HA | CMV promoter, N-terminal HA tag, ampicillin resistance gene | Clontech (Mountain View, USA) |
| pEGFP-N1 | CMV promoter, C-terminal EGFP tag, kanamycin resistance gene | Clontech (Mountain View, USA) |
| pCMV- HA-TDP43 | CMV promoter, N-terminal HA tag fused to *TARDBP* ORF, ampicillin resistance gene | This study |
| pCMV-HA-TDP43-A315T | Identical to pCMV-HA-TDP43 but encodes the p.Ala315Thr variant of TDP-43 | This study |
| pCMV-HA-TDP43-S347P | Identical to pCMV-HA-TDP43 but encodes the p.Ser347Pro variant of TDP-43 | This study |
| pCMV-HA-TDP43-G376V | Identical to pCMV-HA-TDP43 but encodes the p.Gly376Val variant of TDP-43 | This study |
| pEGFP-N1-TDP43 | CMV promoter, C-terminal EGFP tag fused to *TARDBP* ORF, kanamycin resistance gene | This study |
| pEGFP-N1-TDP43-A315T | Identical to pEGFP-N1-TDP43 but encodes the p.Ala315Thr variant of TDP-43 | This study |
| pEGFP-N1-TDP43-S347P | Identical to pEGFP-N1-TDP43 but encodes the p.Ser347Pro variant of TDP-43 | This study |
| pEGFP-N1-TDP43-G376V | Identical to pEGFP-N1-TDP43 but encodes the p.Gly376Val variant of TDP-43 | This study |
| pCMV3-N-HA-TIA1 | CMV promoter, N-terminal HA tag, kanamycin resistance gene (clone HG18574-NY) | Sino Biological, (Eschborn, Germany) |
| pJ4M/TDP-43 | T7 promoter, human *TARDBP* ORF, TEV site, MBP-His6 tag, kanamycin resistance gene (clone 104480) | Addgene (Watertown, USA) |
| pJ4M/TDP-43-G376V | Identical to pJ4M/TDP-43 but encodes the p.Gly376Val variant of TDP-43 | This study |

**Table 10: Primary antibodies**

| Antibody | Host species | Application: Dilution | Supplier |
|---|---|---|---|
| Anti-TDP-43 | Rabbit | WB: 1:1,000 | Proteintech (Rosemont, USA) |
| Anti-GAPDH | Mouse | WB: 1:500 | Merck Millipore (Burlington, USA) |

(table continued on next page)

(table continued from previous page)

| Antibody | Host species | Application: Dilution | Supplier |
|---|---|---|---|
| Anti-GFP | Rabbit | WB: 1:5,000<br>IF: 1:500 | Abcam (Cambridge, UK) |
| Anti-HA | Mouse | WB: 1:1,000<br>IF: 1:500 | Roche (Basel, Switzerland) |

**Table 11: Secondary antibodies**

| Antibody | Host species | Application: Dilution | Supplier |
|---|---|---|---|
| IRDye 680RD Anti-Mouse IgG | Donkey | WB: 1:10,000 | Licor (Lincoln, USA) |
| IRDye 680RD Anti-Rabbit IgG | Donkey | WB: 1:10,000 | Licor (Lincoln, USA) |
| IRDye 800CW Anti-Mouse IgG | Donkey | WB: 1:10,000 | Licor (Lincoln, USA) |
| IRDye 800CW Anti-Rabbit IgG | Donkey | WB: 10,000 | Licor (Lincoln, USA) |
| Alexa Fluor 488 Anti-Rabbit IgG | Goat | IF: 1:500 | Invitrogen, Thermo Fisher (Waltham, USA) |
| Alexa Fluor 594 Anti-Mouse IgG | Goat | IF: 1:500 | Invitrogen, Thermo Fisher (Waltham, USA) |

**Table 12: Bacterial strains and mammalian cell lines**

| Strain/cell line | Description | Supplier |
|---|---|---|
| DH5α | Engineered *E. coli* strain | Sigma-Aldrich (Taufkirchen, Germany) |
| Rosetta 2 DE3 | Engineered *E. coli* strain | Sigma-Aldrich (Taufkirchen, Germany) |
| HEK293 | Human embryonic kidney cell line | ATCC (Manassas, USA) |
| NSC-34 | Mouse motor neuron-like cell line | ATCC (Manassas, USA) |

**Table 13: Software**

| Description | Supplier |
|---|---|
| BioRender | BioRender (Toronto, Canada) |
| ColorSync Utility in macOS | Apple Computer Corporation (Cupertino, USA) |
| GraphPad Prism 9 and 10 | GraphPad Software (La Jolla, USA) |

## 3.2 Molecular biology methods

### 3.2.1 Polymerase chain reaction

Polymerase chain reaction (PCR) amplification of the desired DNA fragments was carried out with AccuPrime Pfx DNA Polymerase (Invitrogen, Thermo Fisher). The corresponding primers (**Table 8**) were custom-ordered from Metabion (Martinsried, Germany). Details of the reaction composition (**Table 14**) and the thermal cycling program (**Table 15**) are provided below.

**Table 14: Composition of PCR mixture**

| Component | Amount |
|---|---|
| DNA template | 10-50 ng |
| dNTPs | 200 µM each |
| 10xAccuPrime Pfx Buffer | 1 µL |
| AccuPrime Pfx DNA Polymerase | 0.4 µL |
| Forward and reverse primers | 100 pmol each |
| Nuclease-free $H_2O$ | ad 50 µL |

**Table 15: PCR cycling conditions**

| Step | Temperature | Duration | Cycles |
|---|---|---|---|
| Initial denaturation | 95°C | 2 min | 1 |
| Denaturation | 95°C | 30 sec | |
| Annealing | 60°C | 30 sec | 35x |
| Elongation | 72°C | 1 min | |
| Final extension | 72°C | 5 min | 1 |

### 3.2.2 Agarose gel electrophoresis and DNA purification

PCR products and restriction digests were run on 1% agarose gels prepared in 1x TAE buffer (40 mM Tris, 20 mM acetic acid, 1 mM EDTA) containing 0.1 µg/mL ethidium bromide. Samples were mixed with 6× DNA loading dye (Thermo Fisher) and electrophoresed at 140 V. DNA bands were visualized under UV illumination, and their sizes compared with GeneRuler 100 bp and 1 kb DNA markers (Thermo Fisher). Bands of the expected length were excised, purified with the NucleoSpin Gel and PCR Clean-up Kit (Macherey-Nagel), and quantified at 260 nm using a NanoDrop 1000 spectrophotometer (Peqlab). Purified DNA was subsequently used for downstream cloning or Sanger sequencing.

### 3.2.3 Generation of mammalian and bacterial TDP-43 expression constructs

Mammalian expression constructs encoding wild-type TDP-43 in pCMV-HA and pEGFP-N1 (Clontech) were generated by PCR amplification of the full-length human *TARDBP* coding sequence from pCMV-SPORT6/TDP-43 (Horizon Discovery). Primers were designed to match the termini of the coding sequence and included restriction sites for cloning (**Table 8**). The amplified fragments were separated on agarose gels, purified, digested with the appropriate restriction endonucleases, and inserted into the pCMV-HA or pEGFP-N1 backbones. Point variants p.Ala315Thr, p.Ser347Pro, and p.Gly376Val were introduced by overlap extension PCR using complementary mismatch primers carrying the desired substitutions (**Table 8**) (66).

Two PCR reactions were performed with pCMV-SPORT6/TDP-43 as template, each combining one mismatch primer with one terminal primer (see above). The resulting overlapping fragments were then combined, extended, and amplified with terminal primers to yield the mutated full-length product. These products were gel-purified, digested with restriction enzymes, and cloned into pCMV-HA or pEGFP-N1. For bacterial expression, the p.Gly376Val variant of TDP-43-TEV-MBP-His6 was generated using the QuikChange mutagenesis system (Agilent), with the wild-type construct pJ4M/TDP-43 (Addgene) as the template. All constructs were verified by Sanger sequencing using standard plasmid primers. **Table 9** lists all constructs used in this study.

### 3.2.4 Restriction digest and ligation

Prior to ligation, gel-purified PCR-derived inserts and plasmid vectors were digested with the corresponding restriction endonucleases. For cloning into pCMV-HA, XhoI and NotI were used, while pEGFP-N1 constructs were prepared using XhoI and HindIII. The digestion mixtures (**Table 16**) were incubated for 1 h at 37 °C, followed by recovery of the DNA fragments through gel extraction.

**Table 16: Composition of restriction digest mixture**

| Component | Amount |
|---|---|
| Plasmid | 2-10 µg |
| Restriction endonucleases | 2.5 µL each |
| 10x CutSmart buffer | 5 µL |
| Nuclease-free $H_2O$ | ad 50 µL |

Insert and vector preparations were then joined with T4 DNA ligase (New England Biolabs) at a molar ratio of 1:3 (vector to insert). Ligation reactions (**Table 17**) were maintained overnight at 16 °C, heat-inactivated at 65 °C for 10 min, and subsequently used for the transformation of bacteria.

**Table 17: Composition of ligation mixture**

| Component | Amount |
|---|---|
| Plasmid | 50-100 ng |
| Insert | 15-80 ng |
| T4 DNA ligase | 1 µL |
| 10x T4 DNA reaction buffer | 1 µL |
| Nuclease-free $H_2O$ | ad 10 µL |

### 3.2.5 Bacterial transformation and colony screening

Competent *E. coli* DH5α cells were transformed with the recombinant plasmids using the calcium chloride protocol (67). Fifty µL of cells were combined with 5 µL of the ligation mix, kept on ice, heat-shocked at 42 °C, briefly chilled again, and then given a 1 h recovery period at 37 °C in LB medium (1% tryptone, 0.5% yeast extract, 1% NaCl, pH 7). Transformed cells were pelleted by centrifugation (13,000 rpm for 1 min), resuspended in 100 µL fresh LB, and plated on LB agar (LB with 20 g/L bacto agar) supplemented with the appropriate antibiotic (100 µg/mL ampicillin or 50 µg/mL kanamycin, depending on the construct), Plates were incubated overnight at 37 °C to allow colony growth. Individual colonies were screened by colony PCR (**Table 18** and **Table 19**), followed by agarose gel electrophoresis of the amplicons. Colonies confirmed to contain the correct insert were subsequently used to start liquid cultures.

**Table 18: Composition of PCR mixture for colony PCR**

| Component | Amount |
|---|---|
| Maxima Hot Start Green Master Mix | 13 µL |
| Template | small portion of *E. coli* colony |
| Two Primers | 1 µL each |
| Nuclease-free $H_2O$ | ad 25 µL |

**Table 19: PCR cycling conditions for colony PCR**

| Step | Temperature | Duration | Cycles |
|---|---|---|---|
| Initial denaturation | 95°C | 6 min | 1 |
| Denaturation | 95°C | 30 sec | |
| Annealing | 55°C | 30 sec | 40x |
| Elongation | 72°C | 1 min | |
| Final extension | 72°C | 7 min | 1 |

### 3.2.6 Liquid culture of transformed bacteria

Colonies that tested positive in colony PCR were expanded in liquid culture. Individual colonies were transferred into LB medium supplemented with the corresponding selective antibiotic and cultured overnight at 37 °C with constant agitation to ensure aeration and optimal bacterial growth. These overnight cultures were used directly for plasmid isolation.

### 3.2.7 Isolation of plasmid DNA

Plasmid DNA was isolated using the NucleoBond PC 500 kit (Macherey-Nagel) according to the manufacturer's recommended procedure. Cell pellets obtained from overnight cultures were resuspended, lysed under alkaline conditions, and neutralized to allow precipitation of genomic DNA and proteins. The clarified lysates were applied to the supplied anion-exchange columns, washed thoroughly to remove residual contaminants, and plasmid DNA was eluted in high-salt buffer. DNA was precipitated with isopropanol, washed with 70% ethanol, air-dried, and resuspended in TE buffer (10 mM Tris-HCl, 1 mM EDTA, pH 7.5). The concentration and purity of the DNA preparations were assessed at 260 nm (NanoDrop 1000, Peqlab). Purified plasmids were verified by Sanger sequencing before use in subsequent experiments.

### 3.2.8 Sanger sequencing

Construct integrity was verified by Sanger sequencing. Both purified PCR amplicons and recombinant plasmids were sent to Eurofins MWG Operon (Ebersberg, Germany) for analysis using the corresponding oligonucleotide primers.

## 3.3 Cell biology methods

### 3.3.1 Maintenance, transient transfection, and harvest of cell cultures

HEK293 and NSC-34 cells were maintained under standard conditions in DMEM (Gibco, Thermo Fisher) supplemented with 10% fetal calf serum, 2 mM L-glutamine, 40 U/mL penicillin, and 0.04 mg/mL streptomycin. Cultures were incubated at 37 °C in a humidified atmosphere containing 5% $CO_2$. Cells were routinely subcultured once they reached approximately 70% confluence. For passaging, monolayers were rinsed with PBS, detached with 0.05% trypsin-EDTA, and reseeded into fresh growth medium at the appropriate dilution. Transient transfections were carried out depending on the cell type. HEK293 cells were transfected with jetPEI (Polyplus), while NSC-34 cells were transfected with Lipofectamine 2000 (Invitrogen, Thermo Fisher). All procedures were performed following the respective supplier protocols. Cells were transfected either with EGFP-tagged *TARDBP* constructs (wild-type or variants) or, in co-transfection experiments, with HA-tagged *TARDBP* constructs together with empty GFP plasmids (to monitor transfection efficiency). At 24-48 h post-transfection, cells were harvested by washing with ice-cold PBS, detachment by scraping, and centrifugation at 13,200 rpm for 8 min at 4 °C.

### 3.3.2 Induction of cellular stress

To model cellular stress, transfected cells were incubated with sodium arsenite (0.5 mM final concentration; Sigma-Aldrich) for 1 h at 37 °C.

### 3.3.3 Cell viability assay

Cell viability was evaluated using the Vybrant MTT Cell Proliferation Assay Kit (Invitrogen, Thermo Fisher). Equal numbers of transfected HEK293 cells were seeded into 96-well plates. Comparable transfection efficiencies of GFP-tagged constructs were confirmed by fluorescence microscopy prior to the assay. Before adding the reagent, the medium was replaced with 100 µL of fresh culture medium per well. Subsequently, 10 µL of 12 mM MTT solution was added to each well and incubated for 4 h at 37 °C, during which metabolically active cells reduced the tetrazolium compound to formazan crystals. These crystals were dissolved by the addition of 100 µL sodium dodecyl sulfate (SDS)-HCl solution, followed by a further 4 h incubation at 37 °C. The solubilized formazan was quantified by measuring absorbance at 570 nm using a TECAN Infinite M200 PRO microplate reader. Cell viability was expressed as the relative absorbance of transfected samples compared to untreated control cells. Values represent means of three technical replicates from two independent experiments.

## 3.4 Protein methods

### 3.4.1 Protein isolation and quantification

Cells harvested as described above were resuspended in 150 µL of ice-cold RIPA buffer (**Table 7**) supplemented with RNase A (54). Cell disruption was achieved by repeatedly passing the suspension ten times through a fine-gauge syringe, followed by a 30-min incubation on ice. Samples were then subjected to sonication using a Bandelin Sonoplus with an MS73 tip (two bursts of 10 s each, separated by a 5 min cooling period on ice). After an additional 5 min on ice, lysates were clarified by centrifugation at 13,200 rpm for 30 min at 4 °C. Supernatants representing soluble protein fractions were transferred to fresh tubes, while the insoluble pellets were resuspended in RIPA buffer containing 2% sarkosyl and 150 mM NaCl. Protein concentrations were determined spectrophotometrically at 280 nm (NanoDrop 1000, Peqlab).

### 3.4.2 SDS-polyacrylamide gel electrophoresis and western blotting

Protein samples were denatured in loading buffer at 98 °C for 5 min, then separated by SDS-polyacrylamide gel electrophoresis (SDS-PAGE) on 4-15% Mini-PROTEAN precast gels (Bio-

Rad). Proteins were electroblotted onto PVDF membranes using the Trans-Blot Turbo system (Bio-Rad). Membranes were blocked in either TBS-T with 5% milk or PBS with 3% BSA for 1 h at room temperature, followed by overnight incubation at 4 °C with primary antibodies: rabbit anti-GFP (Abcam, 1:5,000), mouse anti-HA (Roche, 1:1,000), mouse anti-GAPDH (Merck Millipore, 1:500), or rabbit anti-TDP-43 (Proteintech, 1:1,000) (**Table 10**). After washing three times for 10 min in TBS-T, membranes were incubated for 1 h at room temperature in the dark with IRDye-conjugated secondary antibodies (Licor, 1:10,000 (**Table 11**)). Signals were detected using the Odyssey Fc Imaging System (Licor), and band intensities were quantified by densitometry using ImageStudio software. Ratios of soluble versus insoluble TDP-43 were calculated across three to five independent western blots.

### 3.4.3 Immunoprecipitation

Protein-protein interactions were analyzed using GFP-Trap magnetic agarose beads (ChromoTek). HEK293 cells were co-transfected with 4 µg each of GFP-tagged *TARDBP* constructs (wild-type or p.Gly376Val variant) and HA-tagged TIA1. After 48 h, cells were harvested as described above, washed twice in ice-cold PBS, and resuspended in ice-cold lysis buffer (10 mM Tris-HCl at pH 7.5, 150 mM NaCl, 0.5 mM EDTA, 0.5% NP-40) supplemented with protease inhibitor cocktail (Roche) and 1 mM PMSF. Lysates were left on ice for 30 min with occasional mixing. After lysates were clarified by centrifugation (13,200 rpm for 10 min at 4 °C), a small fraction of the supernatant was reserved as an input control. The remainder was diluted with wash buffer (**Table 7**, final volume 300 µl) and incubated with equilibrated GFP-Trap beads for 1 h at 4 °C under gentle rotation. Beads were separated magnetically, washed three times with buffer, and bound proteins were eluted by boiling in 100 µl of 2x SDS sample buffer (**Table 7**) for 10 min at 95 °C. Eluted proteins were analyzed by SDS-PAGE and immunoblotting using anti-GFP and anti-HA antibodies.

### 3.4.4 Immunofluorescence staining and microscopy

HEK293 and NSC-34 cells were transfected with HA-tagged *TARDBP* constructs and empty GFP plasmids, seeded onto coverslips, and exposed to sodium arsenite where indicated. Cells were fixed in cold methanol, washed three times with TBS, and incubated in blocking buffer (TBS-T containing 10% fish gelatin) for 30 min at room temperature. Primary antibodies, mouse anti-HA (Roche, 1:500) and rabbit anti-GFP (Abcam, 1:500 (**Table 10**)), were diluted in blocking buffer and applied overnight at 4 °C. After three washes with TBS-T, Alexa Fluor-conjugated secondary antibodies (Invitrogen, 1:500 (**Table 11)**) were added for 1 h at room

temperature in the dark. Coverslips were placed on glass slides and sealed with fluorescence mounting medium (Dako) containing 4,6-diamidino-2 phenylindole (DAPI) for counterstaining of nuclei. Images were captured using an Olympus BX61 FluoView FV1000 confocal microscope (60x/1.42 NA objective, 1.5x zoom). At least 100 cells per condition were analyzed across two independent experiments to quantify TDP-43 aggregate localization.

### 3.4.5 Expression and purification of TDP-43-TEV-MBP-His6 fusion proteins

The TDP-43-TEV-MBP-His6 fusion construct contained a solubility-enhancing maltose-binding protein (MBP) tag, a hexahistidine (His6) tag for affinity purification, and a tobacco etch virus (TEV) protease cleavage site for controlled removal of MBP. For protein production, wild-type and p.Gly376Val constructs were transformed into *E. coli* Rosetta 2 DE3 cells and expressed and purified as described previously (68, 69). In brief, bacteria were grown in LB medium containing kanamycin and chloramphenicol at 37 °C with shaking until mid-log phase (OD600 0.5-0.6). Protein expression was induced with 0.5 mM isopropyl β-D-1-thiogalactopyranoside (IPTG), and cultures were incubated overnight at 16 °C. Cells were then resuspended in lysis buffer (**Table 7**) supplemented with RNase A and lysozyme. After disruption by sonication, lysates were cleared by ultracentrifugation (50,000 rcf, 30 min, 4 °C). Proteins were purified using Ni-NTA agarose (Qiagen), washed with lysis buffer, and eluted with elution buffer containing 300 mM imidazole (**Figure 4A**).

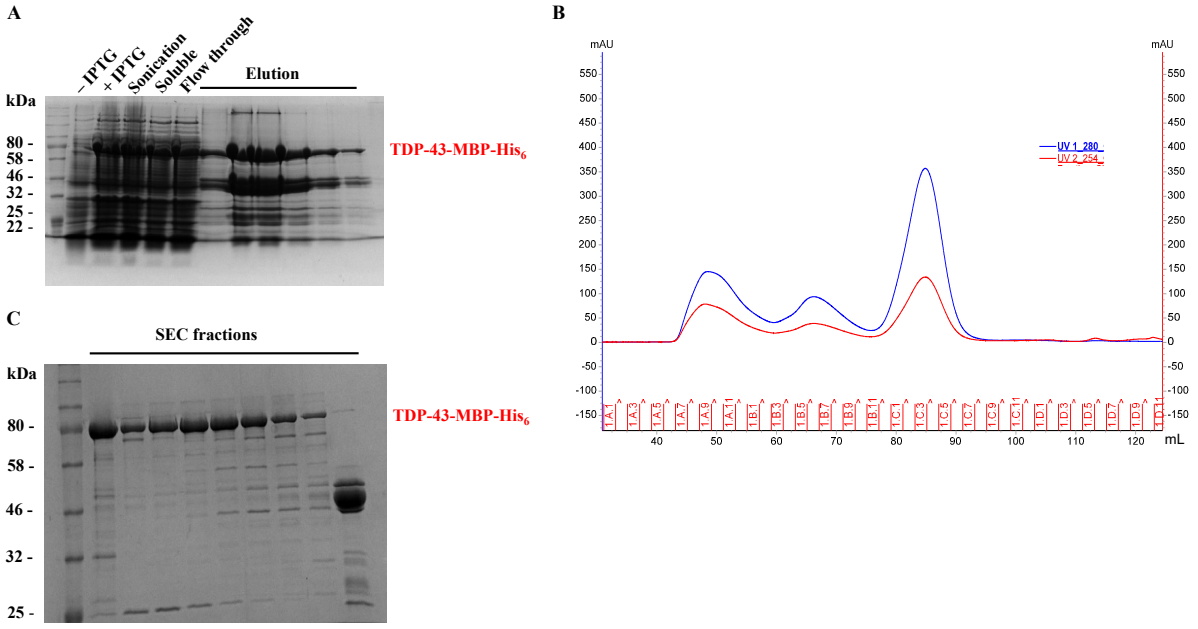


**Figure 4: Purification of p.Gly376Val TDP-43-MBP-His6** (legend continued on next page)

**Figure 4: Purification of p.Gly376Val TDP-43-MBP-His6** (legend continued from previous page)

**A) SDS-PAGE analysis of samples collected during protein purification (Coomassie staining)**
Lanes represent pre-induction (-IPTG), post-induction (+IPTG), post-sonication (sonication), soluble fraction (supernatant), flow-through after washing (flow-through), and eluates from the Ni-NTA agarose beads (elution). Eluates were pooled for size exclusion chromatography (SEC).
**B) SEC profile showing size-based separation**
Absorbance of protein (UV1_280, blue) and nucleic acids (UV2_254, red) is plotted against elution volume (mL).
**C) SDS-PAGE analysis of SEC fractions (Coomassie staining)**
Fractions corresponding to SEC peaks contain oligomeric, monomeric, and cleaved TDP-43-MBP-His6 species.

Further purification by size-exclusion chromatography on a HiLoad 16/600 Superdex 200 pg column (GE Healthcare) separated monomeric TDP-43 fusion proteins from truncated or aggregated protein species (**Figure 4B, C**). Fractions corresponding to the monomeric peak (peak B4-B10) were pooled, concentrated using Amicon Ultra centrifugal filters, aliquoted, snap-frozen, and stored at -80 °C until use in phase separation assays. Protein concentrations were determined by measuring absorbance at 280 nm, using extinction coefficients calculated with ProtParam (70).

## 3.5 Phase separation and aggregation assays

### 3.5.1 Turbidity analysis

Phase separation of recombinant TDP-43 proteins was monitored by turbidity analysis as previously described (68). Briefly, purified TDP-43-TEV-MBP-His6 (wild-type or p.Gly376Val variant) was thawed, resuspended in phosphate buffer (**Table 7**), and cleared by centrifugation (21,000 rcf for 10 min at 4 °C) to remove pre-formed precipitates. Phase separation was initiated by cleavage of the solubilizing MBP tag through the addition of recombinant His6-tagged TEV protease (100 µg/mL, provided by Professor Dormann's group). Immediately after protease addition, samples were transferred into the wells of a 384-well microplate. Following a 30-min incubation at room temperature, turbidity was quantified by measuring absorbance at 600 nm in triplicate using a BioTek PowerWave HT plate reader.

### 3.5.2 Microscopic analysis of condensates

To directly visualize TDP-43 condensate formation, an established microscopy-based assay was employed (68). Briefly, protein samples were prepared as described above and were loaded into µ-Slide 18 Well Flat chambers (Ibidi) pre-coated with Pluronic to minimize surface

adsorption. After a 20-min incubation at room temperature to allow phase separation, samples were imaged by bright-field microscopy. Imaging was performed on an Axio Observer.Z1 inverted wide-field fluorescence microscope equipped with a 63x/1.40 oil immersion objective and an AxioCam506 camera (Zeiss). Images were used to document the number, size, and morphology of condensates formed by wild-type and p.Gly376Val TDP-43.

### 3.5.3 Aggregation kinetics assay

The kinetics of TDP-43 aggregation were examined using semi-denaturing detergent agarose gel electrophoresis (SDD-AGE), following previously published protocols (68). Essentially, the assay involved processing purified wild-type and p.Gly376Val TDP-43 proteins under the same conditions as described above, with the exception that no TEV protease cleavage was performed to retain the MBP-tag. Aliquots were collected at defined time points over five days (days 1-5) and subjected to SDD-AGE. The progressive accumulation of oligomeric and higher-order aggregated species was monitored by western blotting using an anti-TDP-43 antibody.

## 3.6 Statistical analysis

All quantitative data are expressed as mean ± SEM. Statistical analyses were carried out using GraphPad Prism (versions 9 and 10). Fisher's exact test was used for categorical variables. Continuous data were analyzed by one-way analysis of variance (ANOVA), followed by Dunnett's post hoc test for comparisons with the wild-type control, or by two-tailed t-tests with Bonferroni correction for multiple testing. Statistical significance was defined as $p < 0.05$.

# 4 Results

## 4.1 Protein levels and stress-induced insolubility of myopathy-associated TDP-43

Upon overexpression in HEK293 and NSC-34 cells, wild-type TDP-43, as well as ALS- and myopathy-associated variants, produced similar total cellular protein levels, suggesting that the p.Gly376Val and p.Ser347Pro amino acid exchanges did not have a major effect on protein synthesis or stability (**Figure 5**). In line with previous observations, that TDP-43 is primarily a soluble protein under normal physiological conditions but becomes insoluble under cellular stress (50, 71), markedly increased levels of both endogenous TDP-43 and overexpressed wild-type or variant protein were detected in the insoluble fraction of RIPA cell extracts following sodium arsenite-induced stress (**Figure 6**).

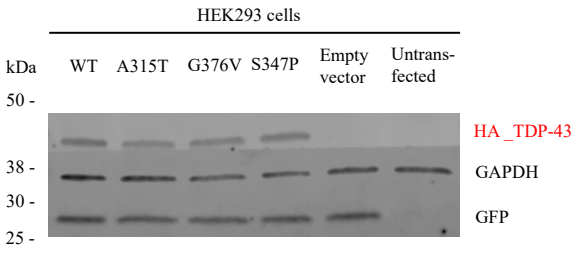


**Figure 5: Protein levels of overexpressed TDP-43**

HEK293 cells were co-transfected with HA-tagged *TARDBP* expression constructs and a GFP expression plasmid. Wild-type and variants displayed similar protein levels. GAPDH was used as a loading control, and GFP served as a transfection efficiency control. kDa, kilodalton.

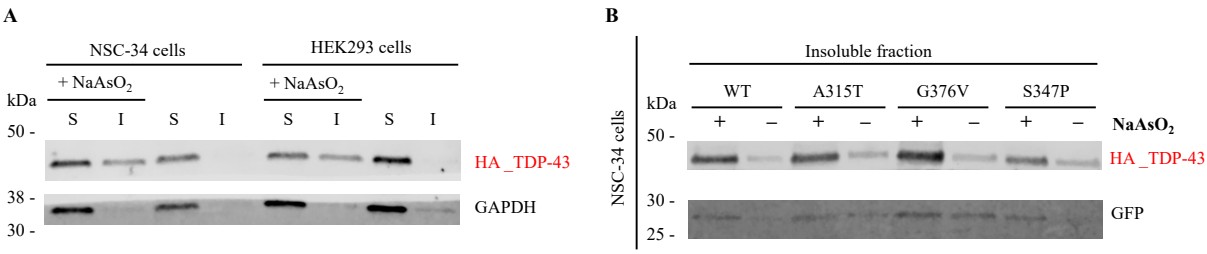


**Figure 6: Stress-induced insolubility of TDP-43**

**A) Western blot of endogenous TDP-43**

Sodium arsenite ($NaAsO_2$)-treated HEK293 and NSC-34 cells exhibited TDP-43 in the insoluble (I) fraction, in addition to the soluble (S) fraction of RIPA cell extracts, whereas untreated cells showed only soluble TDP-43. GAPDH was used as a loading control.

**B) Western blot of overexpressed wild-type and variant TDP-43**

NSC-34 cells were co-transfected with HA-tagged *TARDBP* expression constructs and a GFP vector. The insoluble fraction of RIPA cell extracts was analyzed by western blotting. Regardless of the TDP-43 variant, sodium arsenite ($NaAsO_2$) treatment led to a comparable increase in insoluble TDP-43 levels relative to untreated cells. GFP served as a control for transfection efficiency.

To assess whether the myopathy-associated variants differ from the wild-type in terms of the stress-induced increase in insolubility, TDP-43 solubility was quantified by calculating the ratio of insoluble to soluble fractions (I/S), with values normalized to the wild-type. This analysis revealed comparable solubility profiles across wild-type, myopathy-associated, and ALS-associated TDP-43 (**Figure 7**). Consistent results were obtained in both HEK293 and NSC-34 cells, indicating that the p.Gly376Val and p.Ser347Pro substitutions do not lead to a measurable increase in bulk insolubility under the tested conditions.

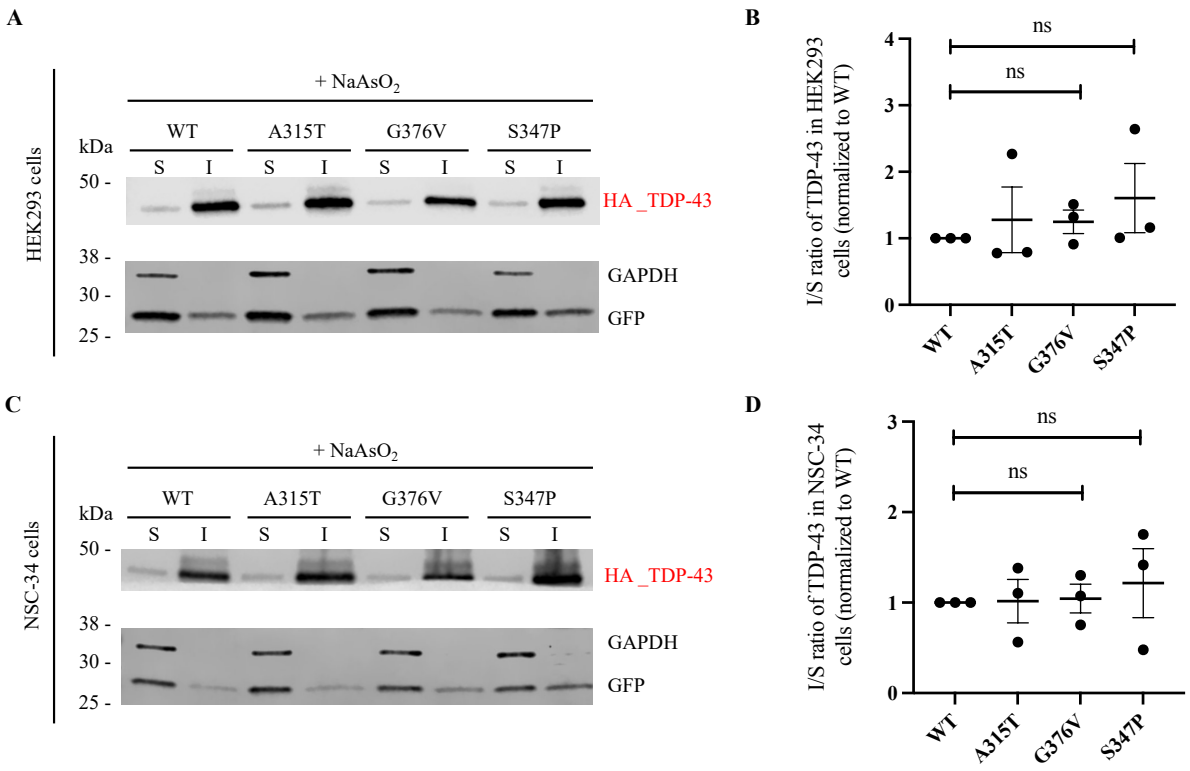


**Figure 7: Quantification of stress-induced TDP-43 insolubility in cell models**

Cells were co-transfected with HA-tagged *TARDBP* constructs and an empty GFP vector. Following sodium arsenite ($NaAsO_2$) treatment, soluble (S) and insoluble (I) fractions were prepared. GAPDH served as a loading and fractionation control, and GFP as a transfection control. TDP-43 solubility was quantified as the insoluble-to-soluble (I/S) ratio normalized to wild-type (mean ± SEM, three replicates). Statistical significance was determined by one-way ANOVA with Dunnett's test (ns = not significant).

**A) Representative western blot of HEK293 cell lysates**

HA-tagged TDP-43 was detected at the expected molecular weight, with all constructs showing stronger signals in the insoluble fraction.

**B) Quantification of TDP-43 solubility in HEK293 cells**

The I/S ratio of TDP-43, normalized to wild-type, was similar across wild-type and variant TDP-43.

**C) Representative western blot of NSC-34 cell lysates**

Consistent with the results obtained in HEK293 cells, TDP-43 was detected in both insoluble and soluble fractions, with a stronger signal observed in the insoluble fraction.

**D) Quantification of TDP-43 solubility in NSC-34 cells**

The I/S ratio of TDP-43, normalized to wild-type, was similar across wild-type and variant TDP-43.

## 4.2 Subcellular localization of myopathy-associated TDP-43

To assess whether myopathy-associated TDP-43 variants alter the subcellular distribution of TDP-43, HEK293 and NSC-34 cells were transiently transfected with HA-tagged constructs expressing either wild-type or variant (p.Gly376Val, p.Ser347Pro, and p.Ala315Thr) TDP-43. Subcellular localization of overexpressed TDP-43 was then determined by confocal immunofluorescence microscopy. Across both cell types, wild-type and variant TDP-43 exhibited a similar range of variable localization patterns. The morphological findings in NSC-34 cells were quantified by categorizing the distribution of TDP-43 as diffuse nuclear staining, nuclear granules, cytoplasmic granules, or mixed patterns (**Figure 8**).

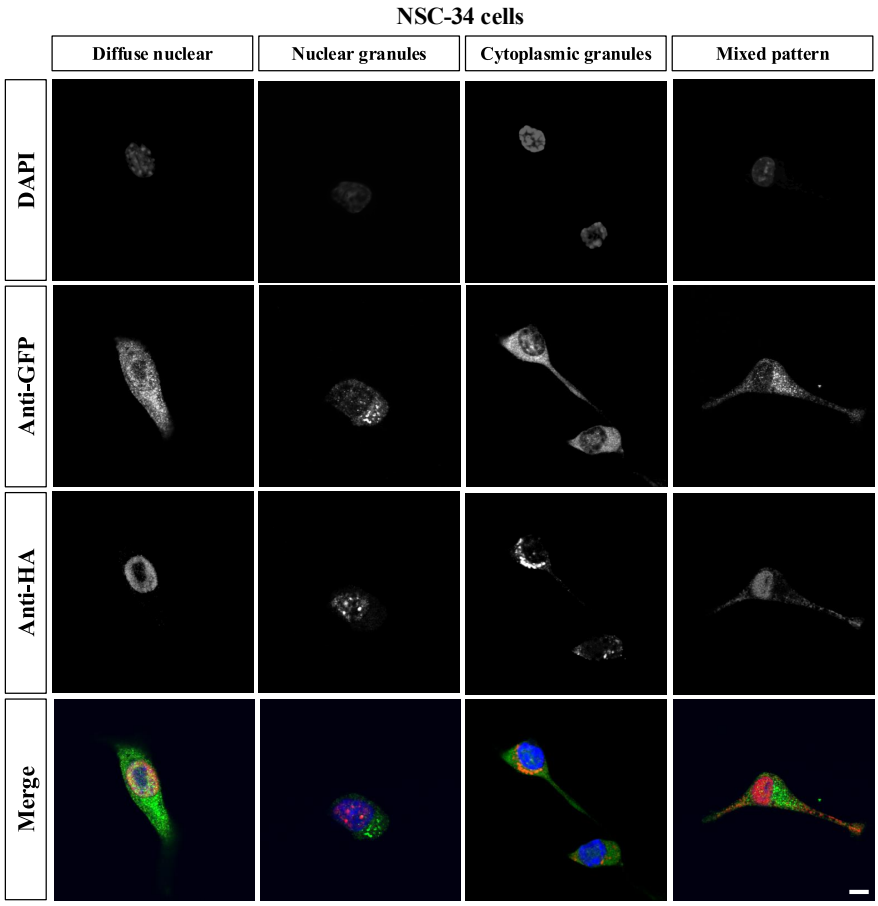


**Figure 8: Subcellular localization of TDP-43**

Representative immunofluorescence images showing the range of TDP-43 subcellular distribution patterns in NSC-34 cells. Observed patterns include diffuse nuclear staining, nuclear granules, cytoplasmic granules, and mixed nuclear-cytoplasmic localization. In the top three rows, individual fluorescence channels are shown in grayscale for enhanced clarity. The merged image (bottom row) displays nuclei stained with DAPI (blue), cytoplasm marked with GFP (green), and HA-tagged TDP-43 detected using an anti-HA antibody (red). Scale bar 10 µm.

Comparative analysis of wild-type and variant TDP-43 overexpression revealed no clear differences in the overall proportion of cells with a granular distribution pattern (**Figure 9A**). However, a higher proportion of cells expressing the myopathy-associated variants showed cytoplasmic TDP-43 granules with absent or strongly reduced nuclear signals. While the increase for p.Gly376Val was not statistically significant compared with wild-type, it was significant for p.Ser347Pro, and both variants exhibited significantly higher proportions than the ALS-associated p.Ala315Thr variant (p.Ser347Pro: 27.7% vs. wild-type 11.8%, $p = 0.0300$; p.Gly376Val: 25.0% vs. p.Ala315Thr: 7.2%, $p = 0.0032$; p.Ser347Pro: 27.7% vs. p.Ala315Thr: 7.2%, $p = 0.0004$; Fisher's exact test with Bonferroni correction) (**Figure 9B**). These findings imply that myopathy-associated variants can alter the subcellular localization of TDP-43.

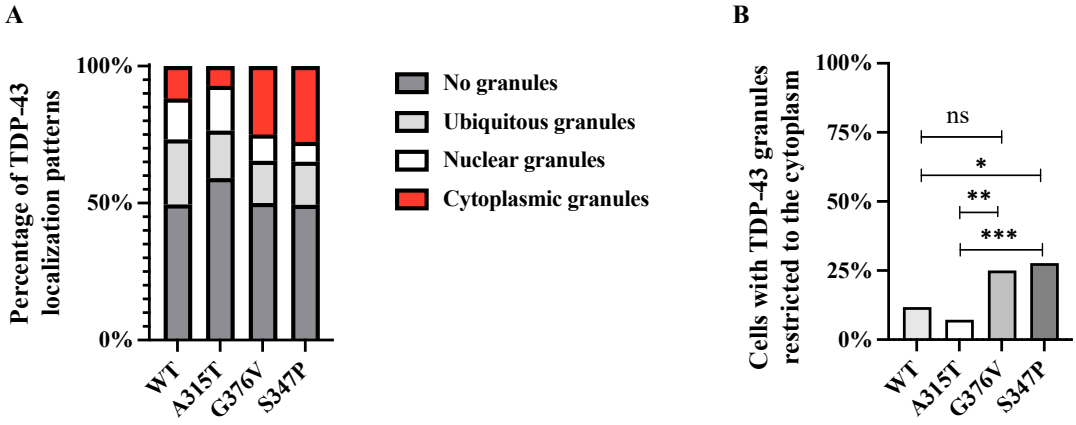


**Figure 9: Quantification of TDP-43 subcellular localization**

NSC-34 cells were transfected with wild-type or variant HA-tagged *TARDBP* expression constructs and analyzed by fluorescence confocal imaging. For each condition, 100 cells were evaluated across two independent experiments.

**A) Distribution of subcellular TDP-43 localization patterns**

While the total number of cells with TDP-43 granules was comparable across conditions, their predominant subcellular localization differed. A distinct increase in cytoplasmic accumulation of TDP-43 granules with concurrent nuclear depletion was observed in cells expressing myopathy-associated *TARDBP* variants compared with cells expressing wild-type or the ALS-associated variant p.Ala315Thr.

**B) Proportions of cells with cytoplasmic TDP-43 granules accompanied by nuclear depletion**

Forced expression of the myopathy-associated variants p.Gly376Val and p.Ser347Pro was associated with a higher proportion of cells exhibiting cytoplasmic TDP-43 granules with loss of nuclear TDP-43 (Fisher's exact test with Bonferroni correction, $*p < 0.05$, $**p < 0.01$, $***p < 0.001$, ns = not significant).

## 4.3 Subcellular localization of myopathy-associated TDP-43 under cellular stress

To assess the subcellular localization and granular pattern formation of TDP-43 under conditions of cellular stress, NSC-34 cells were transfected with expression constructs encoding wild-type and variant HA-tagged TDP-43 and subsequently exposed to sodium arsenite. In

agreement with the data obtained in unstressed cells, a range of distinct subcellular patterns was observed, including diffuse or granular TDP-43 localization within the nucleus, the cytoplasm, or both compartments **(Figure 10)**.

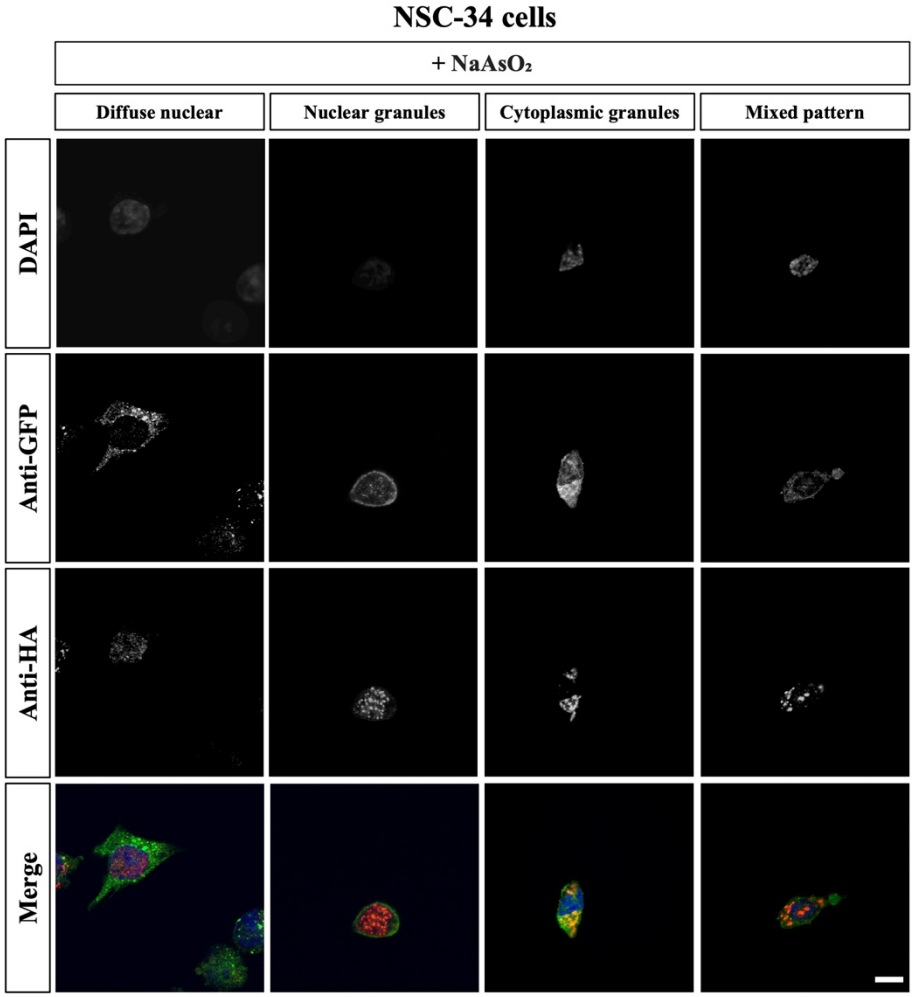


**Figure 10: Subcellular localization of TDP-43 under cellular stress**

Representative immunofluorescence images of sodium arsenite ($NaAsO_2$)-treated NSC-34 cells illustrating the different subcellular TDP-43 localization patterns. Consistent with observations in unstressed cells, TDP-43 was observed in patterns of diffuse nuclear staining, nuclear granules, cytoplasmic granules, and mixed nuclear-cytoplasmic distribution. In the top three rows, individual fluorescence channels are shown in grayscale for enhanced clarity. In the merged image (bottom row), nuclei are stained with DAPI (blue), the cytoplasm is marked by GFP (green), and HA-tagged TDP-43 is detected with an anti-HA antibody (red). Scale bar: 10 µm.

Quantitative analysis showed that cellular stress uniformly increased the proportion of cells with TDP-43-positive granular structures, regardless of the TDP-43 species (**Figure 11A**, compare with **Figure 9A**). As before, the number of cells with only cytoplasmic granular staining accompanied by nuclear depletion was higher for myopathy-associated variants. For p.Gly376Val, the increase reached statistical significance compared with wild-type and the

ALS-associated variant p.Ala315Thr (p.Gly376Val: 24.4% vs. wild-type: 8.1%, $p = 0.0132$; p.Gly376Val: 24.4% vs. p.Ala315Thr: 8.7%, $p = 0.0280$; Fisher's exact test with Bonferroni correction) (**Figure 11B**). Although a similar trend was observed for p.Ser347Pro, the difference was not statistically significant. Reiterating the results from unstressed cells, the experiments further supported the observation that myopathy-associated TDP-43 is associated with redistribution from its physiological nuclear pool toward cytoplasmic granules.

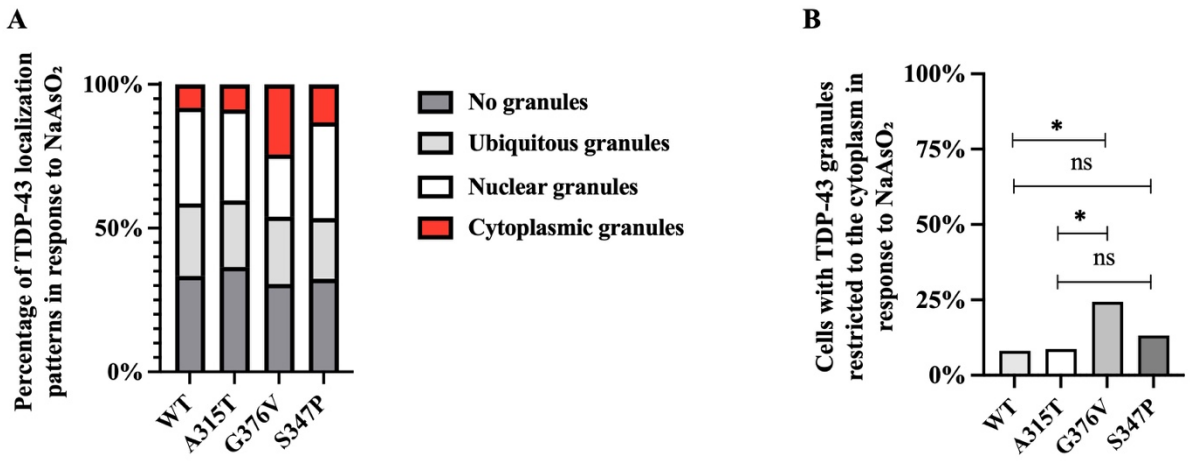


**Figure 11: Quantification of TDP-43 subcellular localization under cellular stress**

NSC-34 cells were transfected with wild-type or variant HA-tagged *TARDBP* expression constructs. Cellular stress was induced by treatment with sodium arsenite ($NaAsO_2$). Cells were then analyzed by fluorescence confocal imaging. For each condition, 100 cells were evaluated across two independent experiments.

**A) Distribution of subcellular TDP-43 localization patterns**

Cellular stress caused a marked increase in the proportion of cells displaying nuclear TDP-43 granules across all conditions (compare with **Figure 9A**). The most pronounced increase in cytoplasmic accumulation of TDP-43 granules with concurrent nuclear depletion was observed in cells expressing the myopathy-associated *TARDBP* variant p.Gly376Val, relative to cells expressing wild-type and the ALS-associated variant p.Ala315Thr. The myopathy-associated variant p.Ser347Pro showed a similar effect to the p.Gly376Val variant; however, the effect was noticeably weaker.

**B) Proportions of cells with cytoplasmic TDP-43 granules and nuclear depletion**

The proportion of cells exhibiting cytoplasmic TDP-43 granules and loss of nuclear TDP-43 signal was significantly higher in cells expressing the p.Gly376Val variant compared with both the wild-type protein and the ALS-associated p.Ala315Thr variant. Although a higher proportion of cells with exclusively cytoplasmic TDP-43 granules was also observed for the p.Ser347Pro variant, this difference was not significant (Fisher's exact test with Bonferroni correction, $*p < 0.05$, ns = not significant).

## 4.4 Phase separation properties of myopathy-associated TDP-43

To more precisely assess the biophysical properties of p.Gly376Val TDP-43, *in vitro* cell-free assays were performed. Purified, bacterially expressed wild-type and p.Gly376Val TDP-43-TEV-MBP-His6 proteins were treated with TEV protease to remove the solubilizing MBP tag,

thereby releasing untagged TDP-43 and initiating phase separation with condensate formation. Spectrophotometric analysis showed a concentration-dependent increase in turbidity for both wild-type and p.Gly376Val TDP-43. Although the variant tended to display higher turbidity at lower concentrations, the difference was not statistically significant, indicating that its phase-separation capacity was not substantially altered (**Figure 12A**). However, bright-field microscopy revealed a marked difference between p.Gly376Val and the wild-type. Wild-type TDP-43 assembled into large, spherical condensates consistent with droplet-like behavior and fusion-driven growth. In contrast, the p.Gly376Val variant formed smaller, irregularly shaped condensates that frequently arranged into chain-like clusters (**Figure 12B**), consistent with a less dynamic, more solid-like material state.

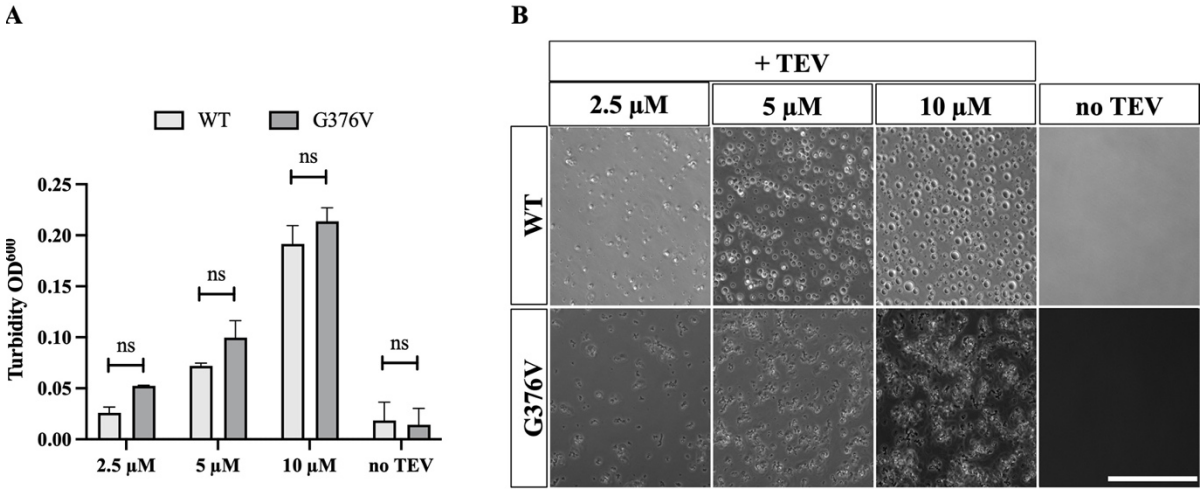


**Figure 12: Spectrophotometric and microscopic analysis of TDP-43 phase separation** (adapted from (62))

TDP-43-TEV-MBP-His6 wild-type and p.Gly376Val were purified from *E. coli*, and phase separation was induced by TEV protease treatment at three TDP-43 concentrations (2.5 µM, 5 µM, 10 µM). In the 'No TEV' control, the MBP tag was retained, thereby preventing TDP-43 phase separation.

**A) Turbidity assay of wild-type and p.Gly376Val TDP-43**

Following induction of phase separation by TEV protease-mediated removal of the solubilizing MBP tag, samples were incubated for 30 minutes prior to measuring optical density at 600 nm. Turbidity increased in a concentration-dependent manner in both wild-type and p.Gly376Val samples. Graphs show data from three independent experiments. Differences were not statistically significant (multiple *t*-tests with Bonferroni correction, ns = not significant).

**B) Representative bright-field images of TDP-43 condensates**

Imaging was performed 20 minutes after induction of phase separation. Wild-type TDP-43 formed large, spherical condensates, while the p.Gly376Val variant produced smaller, irregular condensates often arranged in chain-like clusters. Scale bar: 50 µm.

## 4.5 Aggregation kinetics of myopathy-associated TDP-43

To investigate the aggregation kinetics of TDP-43, TEV protease cleavage was omitted to retain the MBP tag, which slows aggregation and thereby allows the stepwise accumulation of oligomers and higher-order aggregated species to be monitored over several days. Aggregation was assessed by SDD-AGE, which separates soluble monomers from detergent-resistant species that remain stable under semi-denaturing conditions. Over a 5-day incubation, the p.Gly376Val variant showed a markedly accelerated oligomerization process and a greater accumulation of high-molecular-weight, SDS-resistant aggregated species compared with wild-type TDP-43 (**Figure 13**). Thus, the p.Gly376Val substitution accelerates TDP-43 aggregation kinetics and increases the accumulation of higher-order assemblies under *in vitro* conditions.

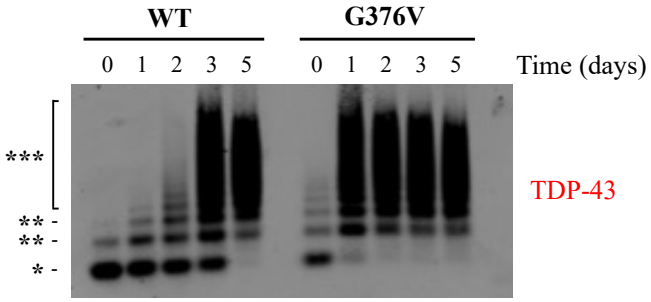


**Figure 13: Time-dependent assembly of detergent-resistant TDP-43 species** (adapted from (62))

Purified recombinant TDP-43-MBP-His6 preparations were incubated for 0-5 days without prior TEV protease treatment. SDD-AGE followed by western blotting with an anti-TDP-43 antibody revealed SDS-resistant, high-molecular-weight species. Bands were assigned as *monomeric, **oligomeric, and ***polymeric TDP-43.

## 4.6 Interaction of myopathy-associated TDP-43 with stress granule protein TIA1

Recruitment of TDP-43 to stress granules – cytoplasmic aggregates that form in response to cellular stress – is facilitated by its interaction with TIA1, a core component of these structures (50). Under pathological conditions, this interaction may contribute to persistent or aberrant stress granule formation, ultimately promoting TDP-43 mislocalization and aggregation (72). Notably, similar to pathogenic variants in *TARDBP*, variants in TIA1 have also been linked to degenerative diseases affecting motor neurons and skeletal muscle (73, 74). To assess whether TDP-43 variants alter interaction with TIA1, co-immunoprecipitation was performed. HEK293 cells were co-transfected with GFP-tagged wild-type or variant TDP-43 constructs together with HA-tagged wild-type TIA1. TDP-43 was immunoprecipitated using anti-GFP antibodies conjugated to agarose beads, and the co-precipitating HA-tagged TIA1 was detected by western

blotting. The myopathy-associated TDP-43 variants interacted with TIA1, and the strength of this interaction appeared comparable to that of wild-type and ALS-associated TDP-43 (**Figure 14**).

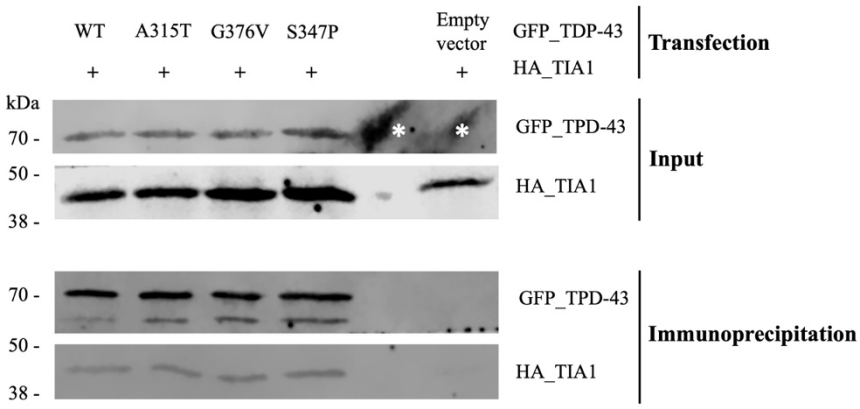


**Figure 14: Co-immunoprecipitation of TDP-43 and TIA1**

Representative western blot of TDP-43/TIA1 co-immunoprecipitation. HEK293 cells were co-transfected with GFP-tagged *TARDBP* constructs and HA-tagged TIA1. Inputs confirmed expression of TDP-43 and HA-TIA1 at comparable levels. Following GFP immunoprecipitation, a TDP-43/TIA1 complex was detected. An empty vector served as a negative control; lane 5 was left empty. White asterisks mark artificial signals from improper handling of the membrane during blotting.

## 4.7 Cellular toxicity of myopathy-associated TDP-43

Previous studies have shown that intracellular accumulation of TDP-43 can induce cytotoxicity and reduce cell viability (48, 75). To examine whether the myopathy-associated TDP-43 variants p.Gly376Val and p.Ser347Pro affect cell viability, HEK293 cells were transiently transfected with GFP-tagged TDP-43 constructs, enabling visualization of transfection efficiency and protein expression by fluorescence microscopy. Cell viability was assessed using the MTT colorimetric assay, which measures metabolic activity as an indirect indicator of viable cell number. No significant differences in cell viability were observed between cells expressing wild-type or variant TDP-43 under the tested conditions (**Figure 15**).

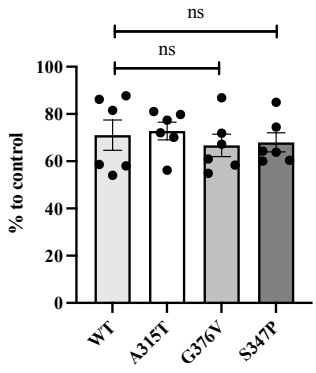


**Figure 15: Viability of TDP-43-overexpressing cells**

HEK293 cells were transfected with GFP-tagged *TARDBP* expression constructs and incubated with MTT and SDS-HCl for four hours. Absorbance was measured at 570 nm and normalized to untransfected controls. Graphs show data from triplicate measurements from two independent experiments. Differences did not reach statistical significance (one-way ANOVA followed by Dunnett's post hoc test, ns, not significant).

# 5 Discussion

TDP-43 is best known for its central role in neurodegeneration, yet growing evidence indicates that it may also contribute to skeletal muscle pathology. Several studies have described cytoplasmic TDP-43 inclusions in muscle tissue of patients with rimmed vacuole myopathies, suggesting that TDP-43 dysfunction is not confined to neurons (58-60). However, unlike in the nervous system, where *TARDBP* variants have long been recognized as a cause of familial ALS, genetic evidence implicating TDP-43 in muscle disease was lacking until recent research identified *TARDBP* variants in individuals with autosomal-dominant distal myopathy (61, 62). The present study investigated the effects of myopathy-associated *TARDBP* variants on the biochemical and cellular properties of TDP-43. By combining several cell-based and *in vitro* approaches, this study elucidates how these variants alter TDP-43 protein properties in ways that may drive disease mechanisms, also revealing parallels with ALS-associated variants. These findings further support the notion of a shared mechanism in TDP-43-related neurodegeneration and myopathy, reinforcing the view that TDP-43 is essential for the integrity of cells and tissues beyond motor neurons and the central nervous system.

## 5.1 Key findings of the study

In overexpression experiments in cell lines, the myopathy-associated p.Gly376Val and p.Ser347Pro variants did not substantially alter the bulk solubility of TDP-43. Cellular stress led to increased levels of both wild-type and variant TDP-43 in the insoluble protein fraction; however, the extent of this stress-induced shift was comparable between wild-type and variant proteins. However, differences became evident when subcellular localization was examined. While wild-type and variant TDP-43 both displayed a spectrum of localization patterns, the variants showed a greater tendency to form cytoplasmic TDP-43-positive granules. This was frequently accompanied by a marked reduction in the diffuse nuclear TDP-43 signal, suggesting a redistribution of the protein from its physiological nuclear pool to cytoplasmic assemblies. Biochemical assays with purified TDP-43 demonstrated that the p.Gly376Val variant disrupted normal condensate formation. While the overall ability of the p.Gly376Val protein to undergo phase separation remained comparable to that of the wild-type, condensate morphology was altered: wild-type TDP-43 assembled into large, spherical, droplet-like structures, whereas the p.Gly376Val variant produced smaller, amorphous condensates with a more solid-like appearance, often arranged in irregular chain-like clusters. These changes in condensate

properties were accompanied by an accelerated accumulation of detergent-resistant oligomers and high-molecular-weight aggregates. Taken together, these findings indicate that myopathy-associated *TARDBP* variants can alter key properties of TDP-43 – including its subcellular distribution, condensate morphology, and aggregation kinetics – in a manner likely to favor a shift toward more solid-like and aggregation-prone states of the protein.

## 5.2 Limitations of the study

The finding that both myopathy-associated *TARDBP* variants did not exhibit a stronger stress-induced increase in bulk insolubility and that p.Gly376Val also retained overall phase separation capacity may appear inconsistent with other results in this study. However, a closer look suggests that this reflects differences in what the assays measure (27, 76, 77). Bulk fractionation in cells and spectrophotometric phase separation assays primarily quantify the distribution of proteins between soluble and insoluble pools or the overall extent of phase separation, but do not capture qualitative or dynamic features such as subcellular distribution, material state, or aggregate formation kinetics. By contrast, localization studies and assays of condensate morphology and formation of detergent-resistant assemblies over time are sensitive to these changes. Differences between cellular and cell-free systems must also be considered. Cells provide buffering mechanisms – such as chaperones and protein clearance pathways (78, 79) – that may delay or prevent the transition of condensates into detergent-insoluble material. Moreover, the definition of ‘insoluble’ depends on the extraction chemistry: for example, RIPA buffer may solubilize early oligomers that SDD-AGE identifies as detergent-resistant (80). Temporal resolution is another factor: SDD-AGE tracks oligomer accumulation over several days, whereas the cellular assays capture only short-term stress responses (1 h sodium arsenite). Finally, assay reproducibility must also be considered: ALS-associated variants have shown variable, sometimes even opposing, effects on TDP-43 solubility, including cases where the same variant yielded different outcomes when tested under slightly modified conditions (50, 81). Notably, a similar observation was made for the myopathy-associated p.Gly376Val variant: it reduced TDP-43 solubility in HEK293 cells after sarkosyl treatment in a collaborator’s experiment (62), but not under sodium arsenite stress in the present work.

A further limitation of the study is that the cellular assays relied on transient transfection and overexpression in non-muscle cell lines (HEK293, NSC-34). Such systems can introduce artifacts, masking endogenous protein behavior (82). In addition, these models lack the skeletal muscle environment, where TDP-43 operates within a distinct molecular context and protein

interactome. More physiologically relevant model systems, for instance, muscle cells derived from induced pluripotent stem cells (iPSCs) or animal models, like p.Gly376Val or p.Ser347Pro knock-in mice, may yield data that more accurately reflect disease mechanisms. It should be noted, however, that mouse models for ALS-associated *TARDBP* variants do not always reliably exhibit a disease phenotype (83, 84). Considering this, the late-onset nature of TDP-43-related myopathy may present even greater challenges for modeling the disease in animals with a short lifespan, likely limiting the observation of age-associated pathological features.

Moreover, this study has not explored the mechanisms underlying p.Gly376Val-induced cytoplasmic mislocalization, altered condensate morphology, and accelerated formation of high-molecular-weight TDP-43 species. Possible contributors include disrupted nuclear transport, impaired RNA binding, altered protein-protein interactions, or changes in post-translational modifications (23). Future work should systematically investigate p.Gly376Val TDP-43's interactions with the nuclear transport machinery and RNA-binding proteins, as well as assess the biophysical properties of p.Gly376Val condensates, particularly their dynamics, material state, and propensity toward irreversible aggregation. It also remains to be determined whether the observed changes in subcellular localization, condensate morphology, and aggregation kinetics are causally related to the pathology. Comprehensive structural and functional analyses will be essential to clarify whether these alterations directly contribute to pathogenesis, represent downstream consequences, or are incidental byproducts of disease progression.

## 5.3 *TARDBP* variants and TDP-43 aggregation

Almost all reported disease-causing *TARDBP* variants, including p.Gly376Val and p.Ser347Pro, lie within the LCD (47). The intrinsically disordered structure of the LCD, characterized by multiple interaction motifs and binding sites, is critical for the phase separation properties of TDP-43, its ability to form intramolecular bonds, and its dynamic interactions with other proteins and RNA molecules (85). Previous studies on ALS-associated variants have shown that such variants can disrupt TDP-43 self-association, promoting the exposure of assembly-driving peptide sequences and eventually leading to pathological aggregation with other TDP-43 molecules (52, 86). The p.Gly376Val substitution likely introduces steric hindrance and increases local hydrophobicity due to valine's bulkier side chain compared to glycine. Similarly, the rigid proline residue introduced by the p.Ser347Pro substitution may distort the local secondary structure, limit backbone flexibility, and promote hydrophobic

interactions. Interestingly, a mutagenesis screen conducted in yeast cells revealed that introducing additional hydrophobic residues into the LCD caused a transition of TDP-43 from dynamic, liquid-like droplets near the nucleus to more static, solid-like deposits in the cytoplasm (87). Similarly, analysis of TDP-43 phase dynamics in HEK293T cells demonstrated that *TARDBP* variants altering local hydrophobicity produced condensates with reduced fluidity and more rigid material properties (29). In line with these findings, the predicted structural alterations introduced by p.Gly376Val and p.Ser347Pro may account for the increased formation of cytoplasmic granules observed upon overexpression of the variants in cells, and may explain the emergence of morphologically distinct p.Gly376Val condensates and accelerated aggregation kinetics. Further investigation using atomistic simulations and coarse-grained modeling could help confirm shifts in hydrophobicity, helicity, and overall folding behavior, providing a more detailed understanding of the structural consequences of these *TARDBP* variants. Additionally, the role of post-translational modifications such as TDP-43 phosphorylation (68), which has been proposed as a protective cellular mechanism to mitigate pathological condensation, could be explored further in the context of these variants.

## 5.4 TDP-43 aggregation and diseases

TDP-43-positive cytoplasmic inclusions arising from abnormal protein aggregation are considered a hallmark of TDP-43 pathology (23). In agreement with this paradigm, immunohistochemical analysis of muscle biopsies from individuals carrying myopathy-associated *TARDBP* variants also revealed sarcoplasmic TDP-43-positive deposits, and experimental data obtained in the present study were consistent with these findings. However, the exact relationship between *TARDBP* variants, aggregate formation, and disease remains incompletely understood (47). Notably, wild-type TDP-43 is inherently aggregation-prone (48). This observation is underscored by the fact that most patients with neurodegenerative diseases associated with TDP-43-positive inclusions have no detectable *TARDBP* variants (46). Thus, pathological aggregation can occur independently of genetic alterations (88). Variants may not directly cause TDP-43 aggregation, but may instead lower the threshold for pathological misfolding, likely acting similarly to as-yet-unknown internal or external triggers that promote aggregation in sporadic cases (47).

Furthermore, distinct *TARDBP* variants can show opposing effects on TDP-43 aggregation and formation of inclusions (89). Adding to this complexity, outcomes of experiments testing TDP-43 solubility and aggregate formation can vary considerably depending on factors such as TDP-

43 expression levels, cellular context, and methodological differences. For instance, while several studies have reported that the known ALS variant p.Ala315Thr enhances TDP-43 aggregation, others have observed unchanged or even reduced cytoplasmic aggregation relative to the wild-type protein (49, 53-55, 75). Finally, the role of TDP-43 aggregation in disease pathology remains a subject of active debate (52, 87). Aggregates may drive disease through toxic gain-of-function mechanisms, reflect a loss of essential nuclear TDP-43 functions, represent inert byproducts of broader cellular dysfunction, or even serve a protective function by sequestering harmful monomeric or oligomeric intermediates (30, 86, 90, 91).

## 5.5 Phenotypic outcome of *TARDBP* variants

Another major unresolved question is why similar *TARDBP* variants – namely, missense variants in the LCD – cause distinct phenotypes, such as myopathy versus ALS. For example, the myopathy-associated p.Ser347Pro variant lies in close proximity to several ALS-associated variants, including p.Asn345Lys (N345K), p.Gly348Cys (G348C), p.Gly348Val (G348V), and p.Gly348Arg (G348R) (40, 92-94). Similarly, p.Gly376Val has been linked to myopathy, whereas p.Gly376Asp (G376D), which affects the same residue but substitutes glycine with aspartic acid instead of valine, causes ALS (95-98). Moreover, the present study demonstrates that the effects of myopathy-associated variants resemble previously reported patterns for ALS-associated TDP-43 variants when analyzed in comparable assays, particularly in terms of mislocalization (48-51, 53, 54) and phase-separation behavior (22, 30, 52). These findings suggest that the specific type, position, or apparent functional consequences of TDP-43 variants do not sufficiently explain phenotypic differences. A definitive genotype-phenotype correlation remains, therefore, elusive. Importantly, variants in other genes have also been linked to both neurodegeneration and myopathy, suggesting that *TARDBP* should be viewed as part of a broader spectrum of multisystem proteinopathies (99).

Future studies should aim to delineate the molecular and cellular mechanisms underlying the heterogeneous phenotypic outcomes of TDP-43 variants. One potential explanation involves molecular determinants of TDP-43 aggregation, such as expression levels, proteostasis capacity, RNA-binding interactions, post-translational modifications, and cellular stress pathways (23). Interindividual differences in how these factors are regulated or function in skeletal muscle versus motor neurons may dictate whether pathology primarily manifests in muscle or in the nervous system. A more speculative, yet intriguing, hypothesis centers on the prion-like features of TDP-43, particularly its capacity for cell-to-cell propagation (100). Under

this model, TDP-43 aggregation may initially arise in skeletal muscle, regardless of whether the clinical phenotype ultimately manifests as myopathy or ALS (101). The aggregation process could then spread to innervating motor neurons, possibly via exosome-mediated transfer (102). In cases where this propagation occurs rapidly, patients may present primarily with ALS, while subclinical or coexisting myopathy is masked by the more severe neurodegenerative process and rapid disease progression. Conversely, slower propagation may lead to the clinical presentation of primary myopathy, with no or only minor signs of motor neuron involvement. Supporting this model, muscle tissue from ALS patients exhibits abnormalities that extend beyond secondary effects of denervation (103, 104), and TDP-43 transgenic mice also develop elevated creatine kinase, myopathic features, and muscle TDP-43 aggregates (105). Furthermore, individuals with TDP-43 myopathy have occasionally developed bulbar symptoms and respiratory compromise in later disease stages, possibly reflecting concomitant or evolving motor neuron involvement.

If confirmed, this model may also have therapeutic implications. Targeting mechanisms that regulate the propagation of TDP-43 - such as exosome-mediated transfer - could potentially prevent or delay progression from a muscle-restricted phenotype to fatal motor neuron disease (106). The development of treatments for TDP-43 proteinopathies remains a major priority, as no causal, mechanism-based therapies are currently available for these progressive, debilitating, and – except for the myopathic form – ultimately fatal conditions. Experimental therapies aimed at modulating TDP-43 expression or aggregation (107) have so far failed to demonstrate clinical benefit despite encouraging preclinical results (108, 109). In light of these setbacks, approaches designed to interfere with cell-to-cell propagation may represent a promising strategy, as they would target a pathogenic mechanism not addressed by previous, unsuccessful attempts.

## 5.6 Conclusion

In summary, *TARDBP* variants associated with myopathy cause changes in TDP-43 subcellular localization, condensate characteristics, and aggregation dynamics. These findings mirror patterns observed in ALS-associated *TARDBP* variants, supporting the notion of a shared underlying disease mechanism driving TDP-43 pathology in both muscle and neuronal tissues. Rather than representing distinct diseases, TDP-43-related myopathic and neurodegenerative phenotypes may reflect two ends of a continuous clinical spectrum. Future research aimed at identifying the determinants responsible for this variable clinical presentation may hold promise for developing targeted therapeutic interventions for TDP-43 proteinopathies.

# 6 Summary

This thesis investigated the effects of two *TARDBP* variants, p.Ser347Pro and p.Gly376Val, linked to late-onset distal myopathy. Although *TARDBP* variants have been intensively studied in the context of neurodegenerative diseases, their role in skeletal muscle pathology remains less well understood. This study employed a combination of cellular models and biochemical assays to examine how these myopathy-associated variants alter the properties of TDP-43, the protein encoded by *TARDBP*, and contribute to disease.

A central finding was that both variants disrupted TDP-43 subcellular localization by promoting the formation of cytoplasmic TDP-43 granules, accompanied by nuclear depletion. *In vitro* assays using purified proteins further demonstrated that the p.Gly376Val variant altered the morphology of TDP-43 condensates formed through phase separation. Unlike the large, spherical droplets produced by wild-type TDP-43, p.Gly376Val formed smaller, amorphous, and irregularly shaped structures. These morphological differences were accompanied by accelerated formation of detergent-resistant oligomers. Several limitations must be taken into account when interpreting these results. Studies of aggregate formation and subcellular localization were conducted in non-muscle cell lines, which, while informative, do not fully reflect the physiological context of skeletal muscle. Furthermore, from a mechanistic standpoint, the specific molecular processes underlying the observed alterations in TDP-43 behavior have yet to be elucidated. It also remains unclear how these changes in TDP-43 are ultimately related to muscle pathology. Lastly, as demonstrated by numerous previous studies in the field of neurodegeneration, experimental outcomes related to TDP-43 biology can vary substantially depending on factors such as expression levels, cellular context, and methodological differences. Despite these limitations, the findings of this thesis indicate that *TARDBP* variants associated with myopathy induce changes in TDP-43 subcellular localization, condensate structure, and aggregation kinetics. Notably, these effects parallel those observed for ALS-associated variants.

This finding supports the existence of shared pathogenic mechanisms and strengthens the view that TDP-43 proteinopathies constitute a continuous clinical spectrum rather than distinct disease entities. Understanding the factors that drive tissue-specific vulnerability to TDP-43 dysfunction may inform the development of targeted therapeutic strategies for these currently untreatable disorders.

# 7 Zusammenfassung

Diese Arbeit untersuchte die Auswirkungen von zwei *TARDBP*-Varianten, p.Ser347Pro und p.Gly376Val, die mit einer spät einsetzenden distalen Myopathie in Verbindung stehen. Obwohl *TARDBP*-Varianten im Zusammenhang mit neurodegenerativen Erkrankungen wie ALS umfangreich erforscht wurden, ist ihre Rolle in der Entstehung von Muskelerkrankungen bisher weniger gut verstanden. Diese Studie verwendete eine Kombination aus Zellkulturexperimenten und biochemischen Analysen, um zu untersuchen, wie Myopathie-assoziierte Varianten die Eigenschaften von TDP-43, dem von *TARDBP* kodierten Protein, verändern und schließlich zum Auftreten der Erkrankung führen.

Beide Varianten führten zu einer veränderten subzellulären Verteilung von TDP-43, charakterisiert durch eine vermehrte Bildung zytoplasmatischer Granula und einen Verlust der nukleären Lokalisation. *In vitro*-Analysen mit gereinigten Proteinen zeigten zudem, dass die p.Gly376Val-Variante die Morphologie von TDP-43-Kondensaten veränderte. Im Gegensatz zu den großen, tropfenartigen Kondensaten, die vom Wildtyp-TDP-43 gebildet werden, zeigte p.Gly376Val kleinere, amorphe und unregelmäßig geformte Strukturen. Diese morphologischen Unterschiede gingen außerdem mit einer beschleunigten Bildung von TDP-43-Oligomeren einher. Bei der Interpretation der Ergebnisse sind mehrere Einschränkungen zu berücksichtigen. Die Untersuchungen zur Aggregatbildung und Lokalisation wurden in Nicht-Muskelzelllinien durchgeführt, die nicht den unmittelbaren physiologischen Kontext von Skelettmuskelgewebe widerspiegeln. Darüber hinaus sind aus mechanistischer Sicht die spezifischen molekularen Mechanismen, die zu den beobachteten Veränderungen der Eigenschaften von TDP-43 führen, noch zu klären. Ebenso ist derzeit noch unklar, wie diese Veränderungen in TDP-43 letztlich mit der Muskelpathologie in Zusammenhang stehen. Schließlich ist aus zahlreichen Studien zu TDP-43 in neurodegenerativen Erkrankungen gut bekannt, dass experimentelle Ergebnisse zur TDP-43-Biologie aufgrund von Faktoren wie Expressionsniveau, Zellkontext und methodischen Unterschieden erheblich variieren können. Trotz dieser Einschränkungen zeigen die Ergebnisse dieser Arbeit, dass Myopathie-assoziierte *TARDBP*-Varianten Veränderungen der subzellulären Lokalisation von TDP-43-Ablagerungen, der Morphologie von TDP-43-Kondensaten und der Dynamik des Aggregationsprozesses bewirken. Bemerkenswerterweise ähneln diese Effekte denen, die bei ALS-assoziierten Varianten beobachtet wurden.

Diese Beobachtung legt die Existenz gemeinsamer pathogenetischer Mechanismen nahe und untermauert das Konzept, dass TDP-43-Proteinopathien ein kontinuierliches klinisches

Spektrum darstellen und keine klar voneinander abgegrenzten Krankheitsentitäten sind. Die Identifizierung von Faktoren, die die gewebespezifische Anfälligkeit für eine TDP-43-Dysfunktion bestimmen, könnte die Entwicklung gezielter therapeutischer Strategien für diese bislang nicht behandelbaren Erkrankungen fördern.

# Bibliography

1. Gowers W. A lecture on myopathy and a distal form: delivered at the National Hospital for the Paralysed and Epileptic. . Br Med J. 1902(2:89-92. https://doi.org/10.1136/bmj.2.2167.89).
2. Kraya T, Zierz S. Distal myopathies: from clinical classification to molecular understanding. Journal of Neural Transmission. 2013;120(1):3-7.
3. Welander L. Myopathia distalis tarda hereditaria; 249 examined cases in 72 pedigrees. Acta Med Scand Suppl. 1951;265:1-124.
4. Liu J, Aoki M, Illa I, Wu C, Fardeau M, Angelini C, et al. Dysferlin, a novel skeletal muscle gene, is mutated in Miyoshi myopathy and limb girdle muscular dystrophy. Nat Genet. 1998;20(1):31-6.
5. Benarroch L, Bonne G, Rivier F, Hamroun D. The 2021 version of the gene table of neuromuscular disorders (nuclear genome). Neuromuscul Disord. 2020;30(12):1008-48.
6. Felice KJ. Distal Myopathies. Neurol Clin. 2020;38(3):637-59.
7. Norwood FL, Harling C, Chinnery PF, Eagle M, Bushby K, Straub V. Prevalence of genetic muscle disease in Northern England: in-depth analysis of a muscle clinic population. Brain : a journal of neurology. 2009;132(Pt 11):3175-86.
8. Udd B. Distal myopathies--new genetic entities expand diagnostic challenge. Neuromuscul Disord. 2012;22(1):5-12.
9. Milone M, Liewluck T. The unfolding spectrum of inherited distal myopathies. Muscle Nerve. 2019;59(3):283-94.
10. Savarese M, Sarparanta J, Vihola A, Jonson PH, Johari M, Rusanen S, et al. Panorama of the distal myopathies. Acta Myol. 2020;39(4):245-65.
11. Deschauer M. Diagnostik von Myopathien, S1-Leitlinie. Deutsche Gesellschaft für Neurologie (Hrsg), Leitlinien für Diagnostik und Therapie in der Neurologie, wwwdgnorg/leitlinien (last access 27092023). 2021.
12. Savarese M, Jokela M, Udd B. Distal myopathy. Handb Clin Neurol. 2023;195:497-519.
13. Zanoteli E, França MC, Jr., Marques W, Jr. Gene-based therapies for neuromuscular disorders. Arq Neuropsiquiatr. 2024;82(6):1-10.
14. Chiò A, Logroscino G, Traynor BJ, Collins J, Simeone JC, Goldstein LA, et al. Global epidemiology of amyotrophic lateral sclerosis: a systematic review of the published literature. Neuroepidemiology. 2013;41(2):118-30.
15. Kiernan MC, Vucic S, Cheah BC, Turner MR, Eisen A, Hardiman O, et al. Amyotrophic lateral sclerosis. Lancet. 2011;377(9769):942-55.
16. Ou SH, Wu F, Harrich D, García-Martínez LF, Gaynor RB. Cloning and characterization of a novel cellular protein, TDP-43, that binds to human immunodeficiency virus type 1 TAR DNA sequence motifs. J Virol. 1995;69(6):3584-96.
17. Buratti E, Baralle FE. Characterization and functional implications of the RNA binding properties of nuclear factor TDP-43, a novel splicing regulator of CFTR exon 9. J Biol Chem. 2001;276(39):36337-43.
18. Ayala YM, De Conti L, Avendaño-Vázquez SE, Dhir A, Romano M, D'Ambrogio A, et al. TDP-43 regulates its mRNA levels through a negative feedback loop. Embo j. 2011;30(2):277-88.
19. Buratti E, Baralle FE. The multiple roles of TDP-43 in pre-mRNA processing and gene expression regulation. RNA Biol. 2010;7(4):420-9.
20. Wang HY, Wang IF, Bose J, Shen CK. Structural diversity and functional implications of the eukaryotic TDP gene family. Genomics. 2004;83(1):130-9.
21. Cushman M, Johnson BS, King OD, Gitler AD, Shorter J. Prion-like disorders: blurring the divide between transmissibility and infectivity. J Cell Sci. 2010;123(Pt 8):1191-201.

22. Conicella AE, Dignon GL, Zerze GH, Schmidt HB, D'Ordine AM, Kim YC, et al. TDP-43 α-helical structure tunes liquid–liquid phase separation and function. Proceedings of the National Academy of Sciences. 2020;117(11):5883-94.
23. Tziortzouda P, Van Den Bosch L, Hirth F. Triad of TDP43 control in neurodegeneration: autoregulation, localization and aggregation. Nat Rev Neurosci. 2021;22(4):197-208.
24. Ayala YM, Zago P, D'Ambrogio A, Xu YF, Petrucelli L, Buratti E, et al. Structural determinants of the cellular localization and shuttling of TDP-43. J Cell Sci. 2008;121(Pt 22):3778-85.
25. Winton MJ, Igaz LM, Wong MM, Kwong LK, Trojanowski JQ, Lee VM. Disturbance of nuclear and cytoplasmic TAR DNA-binding protein (TDP-43) induces disease-like redistribution, sequestration, and aggregate formation. J Biol Chem. 2008;283(19):13302-9.
26. Mackenzie IR, Rademakers R, Neumann M. TDP-43 and FUS in amyotrophic lateral sclerosis and frontotemporal dementia. Lancet Neurol. 2010;9(10):995-1007.
27. Molliex A, Temirov J, Lee J, Coughlin M, Kanagaraj AP, Kim HJ, et al. Phase separation by low complexity domains promotes stress granule assembly and drives pathological fibrillization. Cell. 2015;163(1):123-33.
28. Alberti S, Dormann D. Liquid-Liquid Phase Separation in Disease. Annu Rev Genet. 2019;53:171-94.
29. Schmidt HB, Barreau A, Rohatgi R. Phase separation-deficient TDP43 remains functional in splicing. Nature Communications. 2019;10(1):4890.
30. French RL, Grese ZR, Aligireddy H, Dhavale DD, Reeb AN, Kedia N, et al. Detection of TAR DNA-binding protein 43 (TDP-43) oligomers as initial intermediate species during aggregate formation. J Biol Chem. 2019;294(17):6696-709.
31. Neumann M, Sampathu DM, Kwong LK, Truax AC, Micsenyi MC, Chou TT, et al. Ubiquitinated TDP-43 in frontotemporal lobar degeneration and amyotrophic lateral sclerosis. Science. 2006;314(5796):130-3.
32. Arai T, Hasegawa M, Akiyama H, Ikeda K, Nonaka T, Mori H, et al. TDP-43 is a component of ubiquitin-positive tau-negative inclusions in frontotemporal lobar degeneration and amyotrophic lateral sclerosis. Biochem Biophys Res Commun. 2006;351(3):602-11.
33. Amador-Ortiz C, Lin WL, Ahmed Z, Personett D, Davies P, Duara R, et al. TDP-43 immunoreactivity in hippocampal sclerosis and Alzheimer's disease. Ann Neurol. 2007;61(5):435-45.
34. Josephs KA, Murray ME, Whitwell JL, Parisi JE, Petrucelli L, Jack CR, et al. Staging TDP-43 pathology in Alzheimer's disease. Acta Neuropathol. 2014;127(3):441-50.
35. Arai T, Mackenzie IR, Hasegawa M, Nonoka T, Niizato K, Tsuchiya K, et al. Phosphorylated TDP-43 in Alzheimer's disease and dementia with Lewy bodies. Acta Neuropathol. 2009;117(2):125-36.
36. Chanson JB, Echaniz-Laguna A, Vogel T, Mohr M, Benoilid A, Kaltenbach G, et al. TDP43-positive intraneuronal inclusions in a patient with motor neuron disease and Parkinson's disease. Neurodegener Dis. 2010;7(4):260-4.
37. Schwab C, Arai T, Hasegawa M, Yu S, McGeer PL. Colocalization of transactivation-responsive DNA-binding protein 43 and huntingtin in inclusions of Huntington disease. J Neuropathol Exp Neurol. 2008;67(12):1159-65.
38. Forman MS, Trojanowski JQ, Lee VM. TDP-43: a novel neurodegenerative proteinopathy. Curr Opin Neurobiol. 2007;17(5):548-55.
39. de Boer EMJ, Orie VK, Williams T, Baker MR, De Oliveira HM, Polvikoski T, et al. TDP-43 proteinopathies: a new wave of neurodegenerative diseases. J Neurol Neurosurg Psychiatry. 2020;92(1):86-95.

40. Kabashi E, Valdmanis PN, Dion P, Spiegelman D, McConkey BJ, Vande Velde C, et al. TARDBP mutations in individuals with sporadic and familial amyotrophic lateral sclerosis. Nat Genet. 2008;40(5):572-4.
41. Gitcho MA, Baloh RH, Chakraverty S, Mayo K, Norton JB, Levitch D, et al. TDP-43 A315T mutation in familial motor neuron disease. Ann Neurol. 2008;63(4):535-8.
42. Sreedharan J, Blair IP, Tripathi VB, Hu X, Vance C, Rogelj B, et al. TDP-43 mutations in familial and sporadic amyotrophic lateral sclerosis. Science. 2008;319(5870):1668-72.
43. Borroni B, Bonvicini C, Alberici A, Buratti E, Agosti C, Archetti S, et al. Mutation within TARDBP leads to frontotemporal dementia without motor neuron disease. Hum Mutat. 2009;30(11):E974-83.
44. Brouwers N, Bettens K, Gijselinck I, Engelborghs S, Pickut BA, Van Miegroet H, et al. Contribution of TARDBP to Alzheimer's disease genetic etiology. J Alzheimers Dis. 2010;21(2):423-30.
45. Rayaprolu S, Fujioka S, Traynor S, Soto-Ortolaza AI, Petrucelli L, Dickson DW, et al. TARDBP mutations in Parkinson's disease. Parkinsonism Relat Disord. 2013;19(3):312-5.
46. Lattante S, Rouleau GA, Kabashi E. TARDBP and FUS mutations associated with amyotrophic lateral sclerosis: summary and update. Hum Mutat. 2013;34(6):812-26.
47. Buratti E. Functional Significance of TDP-43 Mutations in Disease. Adv Genet. 2015;91:1-53.
48. Johnson BS, Snead D, Lee JJ, McCaffery JM, Shorter J, Gitler AD. TDP-43 is intrinsically aggregation-prone, and amyotrophic lateral sclerosis-linked mutations accelerate aggregation and increase toxicity. J Biol Chem. 2009;284(30):20329-39.
49. Kabashi E, Lin L, Tradewell ML, Dion PA, Bercier V, Bourgouin P, et al. Gain and loss of function of ALS-related mutations of TARDBP (TDP-43) cause motor deficits in vivo. Hum Mol Genet. 2010;19(4):671-83.
50. Liu-Yesucevitz L, Bilgutay A, Zhang YJ, Vanderweyde T, Citro A, Mehta T, et al. Tar DNA binding protein-43 (TDP-43) associates with stress granules: analysis of cultured cells and pathological brain tissue. PLoS One. 2010;5(10):e13250.
51. Dewey CM, Cenik B, Sephton CF, Dries DR, Mayer P, 3rd, Good SK, et al. TDP-43 is directed to stress granules by sorbitol, a novel physiological osmotic and oxidative stressor. Mol Cell Biol. 2011;31(5):1098-108.
52. Conicella AE, Zerze GH, Mittal J, Fawzi NL. ALS Mutations Disrupt Phase Separation Mediated by α-Helical Structure in the TDP-43 Low-Complexity C-Terminal Domain. Structure. 2016;24(9):1537-49.
53. Barmada SJ, Skibinski G, Korb E, Rao EJ, Wu JY, Finkbeiner S. Cytoplasmic mislocalization of TDP-43 is toxic to neurons and enhanced by a mutation associated with familial amyotrophic lateral sclerosis. J Neurosci. 2010;30(2):639-49.
54. Guo W, Chen Y, Zhou X, Kar A, Ray P, Chen X, et al. An ALS-associated mutation affecting TDP-43 enhances protein aggregation, fibril formation and neurotoxicity. Nat Struct Mol Biol. 2011;18(7):822-30.
55. Estes PS, Boehringer A, Zwick R, Tang JE, Grigsby B, Zarnescu DC. Wild-type and A315T mutant TDP-43 exert differential neurotoxicity in a Drosophila model of ALS. Hum Mol Genet. 2011;20(12):2308-21.
56. Weihl CC, Temiz P, Miller SE, Watts G, Smith C, Forman M, et al. TDP-43 accumulation in inclusion body myopathy muscle suggests a common pathogenic mechanism with frontotemporal dementia. J Neurol Neurosurg Psychiatry. 2008;79(10):1186-9.
57. Hernandez Lain A, Millecamps S, Dubourg O, Salachas F, Bruneteau G, Lacomblez L, et al. Abnormal TDP-43 and FUS proteins in muscles of sporadic IBM: similarities in a TARDBP-linked ALS patient. J Neurol Neurosurg Psychiatry. 2011;82(12):1414-6.

58. Olivé M, Janué A, Moreno D, Gámez J, Torrejón-Escribano B, Ferrer I. TAR DNA-Binding protein 43 accumulation in protein aggregate myopathies. J Neuropathol Exp Neurol. 2009;68(3):262-73.
59. Küsters B, van Hoeve BJ, Schelhaas HJ, Ter Laak H, van Engelen BG, Lammens M. TDP-43 accumulation is common in myopathies with rimmed vacuoles. Acta Neuropathol. 2009;117(2):209-11.
60. Salajegheh M, Pinkus JL, Taylor JP, Amato AA, Nazareno R, Baloh RH, et al. Sarcoplasmic redistribution of nuclear TDP-43 in inclusion body myositis. Muscle Nerve. 2009;40(1):19-31.
61. Ervilha Pereira P, Schuermans N, Meylemans A, LeBlanc P, Versluys L, Copley KE, et al. C-terminal frameshift variant of TDP-43 with pronounced aggregation-propensity causes rimmed vacuole myopathy but not ALS/FTD. Acta Neuropathologica. 2023.
62. Zibold J, Lessard LER, Picard F, da Silva LG, Zadorozhna Y, Streichenberger N, et al. The new missense G376V-TDP-43 variant induces late-onset distal myopathy but not amyotrophic lateral sclerosis. Brain : a journal of neurology. 2023.
63. Bonifacino J, Dasso M, Harford J, Lippincott-Schwartz J, Yamada K. Current Protocols in Cell Biology. Hoboken, NJ, USA: John Wiley & Sons, Inc.; 2001 2001-05-15.
64. Ausubel FM, Brent, R., Kingston, R. E., Moore, D. D., Seidman, J. G., Smith, J. A., & Struhl, K. Current protocols in molecular biology. New York 1997.
65. Sambrook J, Fritsch, E. R., & Maniatis, T. Molecular Cloning: A Laboratory Manual. Cold Spring Harbor, New York Cold Spring Harbor Laboratory Press; 1989.
66. Ho SN, Hunt HD, Horton RM, Pullen JK, Pease LR. Site-directed mutagenesis by overlap extension using the polymerase chain reaction. Gene. 1989;77(1):51-9.
67. Dagert M, Ehrlich SD. Prolonged incubation in calcium chloride improves the competence of Escherichia coli cells. Gene. 1979;6(1):23-8.
68. Gruijs da Silva LA, Simonetti F, Hutten S, Riemenschneider H, Sternburg EL, Pietrek LM, et al. Disease-linked TDP-43 hyperphosphorylation suppresses TDP-43 condensation and aggregation. Embo j. 2022;41(8):e108443.
69. Hutten S, Usluer S, Bourgeois B, Simonetti F, Odeh HM, Fare CM, et al. Nuclear Import Receptors Directly Bind to Arginine-Rich Dipeptide Repeat Proteins and Suppress Their Pathological Interactions. Cell Rep. 2020;33(12):108538.
70. Gasteiger E, Gattiker A, Hoogland C, Ivanyi I, Appel RD, Bairoch A. ExPASy: The proteomics server for in-depth protein knowledge and analysis. Nucleic Acids Res. 2003;31(13):3784-8.
71. Liu R, Yang G, Nonaka T, Arai T, Jia W, Cynader MS. Reducing TDP-43 aggregation does not prevent its cytotoxicity. Acta Neuropathol Commun. 2013;1:49.
72. McDonald KK, Aulas A, Destroismaisons L, Pickles S, Beleac E, Camu W, et al. TAR DNA-binding protein 43 (TDP-43) regulates stress granule dynamics via differential regulation of G3BP and TIA-1. Hum Mol Genet. 2011;20(7):1400-10.
73. Hackman P, Sarparanta J, Lehtinen S, Vihola A, Evilä A, Jonson PH, et al. Welander distal myopathy is caused by a mutation in the RNA-binding protein TIA1. Ann Neurol. 2013;73(4):500-9.
74. Mackenzie IR, Nicholson AM, Sarkar M, Messing J, Purice MD, Pottier C, et al. TIA1 Mutations in Amyotrophic Lateral Sclerosis and Frontotemporal Dementia Promote Phase Separation and Alter Stress Granule Dynamics. Neuron. 2017;95(4):808-16.e9.
75. Wang X, Zhou S, Ding X, Ma M, Zhang J, Zhou Y, et al. Activation of ER Stress and Autophagy Induced by TDP-43 A315T as Pathogenic Mechanism and the Corresponding Histological Changes in Skin as Potential Biomarker for ALS with the Mutation. Int J Biol Sci. 2015;11(10):1140-9.
76. Patel A, Malinovska L, Saha S, Wang J, Alberti S, Krishnan Y, et al. ATP as a biological hydrotrope. Science. 2017;356(6339):753-6.

77. Zhang L, Trushin S, Christensen TA, Tripathi U, Hong C, Geroux RE, et al. Differential effect of amyloid beta peptides on mitochondrial axonal trafficking depends on their state of aggregation and binding to the plasma membrane. Neurobiol Dis. 2018;114:1-16.
78. Maharana S, Wang J, Papadopoulos DK, Richter D, Pozniakovsky A, Poser I, et al. RNA buffers the phase separation behavior of prion-like RNA binding proteins. Science. 2018;360(6391):918-21.
79. Balch WE, Morimoto RI, Dillin A, Kelly JW. Adapting proteostasis for disease intervention. Science. 2008;319(5865):916-9.
80. Imomnazarov K, Lopez-Scarim J, Bagheri I, Joers V, Tansey MG, Martín-Peña A. Biochemical fractionation of human α-Synuclein in a Drosophila model of synucleinopathies. bioRxiv. 2024.
81. Watanabe S, Kaneko K, Yamanaka K. Accelerated disease onset with stabilized familial amyotrophic lateral sclerosis (ALS)-linked mutant TDP-43 proteins. J Biol Chem. 2013;288(5):3641-54.
82. Stepanenko AA, Heng HH. Transient and stable vector transfection: Pitfalls, off-target effects, artifacts. Mutat Res Rev Mutat Res. 2017;773:91-103.
83. Watanabe S, Oiwa K, Murata Y, Komine O, Sobue A, Endo F, et al. ALS-linked TDP-43(M337V) knock-in mice exhibit splicing deregulation without neurodegeneration. Mol Brain. 2020;13(1):8.
84. Huang SL, Wu LS, Lee M, Chang CW, Cheng WC, Fang YS, et al. A robust TDP-43 knock-in mouse model of ALS. Acta Neuropathol Commun. 2020;8(1):3.
85. Pakravan D, Michiels E, Bratek-Skicki A, De Decker M, Van Lindt J, Alsteens D, et al. Liquid-Liquid Phase Separation Enhances TDP-43 LCD Aggregation but Delays Seeded Aggregation. Biomolecules. 2021;11(4).
86. Guenther EL, Cao Q, Trinh H, Lu J, Sawaya MR, Cascio D, et al. Atomic structures of TDP-43 LCD segments and insights into reversible or pathogenic aggregation. Nat Struct Mol Biol. 2018;25(6):463-71.
87. Bolognesi B, Faure AJ, Seuma M, Schmiedel JM, Tartaglia GG, Lehner B. The mutational landscape of a prion-like domain. Nat Commun. 2019;10(1):4162.
88. Budini M, Buratti E, Morselli E, Criollo A. Autophagy and Its Impact on Neurodegenerative Diseases: New Roles for TDP-43 and C9orf72. Front Mol Neurosci. 2017;10:170.
89. Jiang LL, Zhao J, Yin XF, He WT, Yang H, Che MX, et al. Two mutations G335D and Q343R within the amyloidogenic core region of TDP-43 influence its aggregation and inclusion formation. Sci Rep. 2016;6:23928.
90. Walker AK, Spiller KJ, Ge G, Zheng A, Xu Y, Zhou M, et al. Functional recovery in new mouse models of ALS/FTLD after clearance of pathological cytoplasmic TDP-43. Acta Neuropathol. 2015;130(5):643-60.
91. Johnson BS, McCaffery JM, Lindquist S, Gitler AD. A yeast TDP-43 proteinopathy model: Exploring the molecular determinants of TDP-43 aggregation and cellular toxicity. Proc Natl Acad Sci U S A. 2008;105(17):6439-44.
92. Rutherford NJ, Zhang YJ, Baker M, Gass JM, Finch NA, Xu YF, et al. Novel mutations in TARDBP (TDP-43) in patients with familial amyotrophic lateral sclerosis. PLoS Genet. 2008;4(9):e1000193.
93. Kirby J, Goodall EF, Smith W, Highley JR, Masanzu R, Hartley JA, et al. Broad clinical phenotypes associated with TAR-DNA binding protein (TARDBP) mutations in amyotrophic lateral sclerosis. Neurogenetics. 2010;11(2):217-25.
94. Ticozzi N, LeClerc AL, van Blitterswijk M, Keagle P, McKenna-Yasek DM, Sapp PC, et al. Mutational analysis of TARDBP in neurodegenerative diseases. Neurobiol Aging. 2011;32(11):2096-9.

95. Conforti FL, Sproviero W, Simone IL, Mazzei R, Valentino P, Ungaro C, et al. TARDBP gene mutations in south Italian patients with amyotrophic lateral sclerosis. Journal of Neurology, Neurosurgery & Psychiatry. 2011;82(5):587-8.
96. Czell D, Andersen PM, Morita M, Neuwirth C, Perren F, Weber M. Phenotypes in Swiss patients with familial ALS carrying TARDBP mutations. Neurodegener Dis. 2013;12(3):150-5.
97. Nishiyama A, Niihori T, Warita H, Izumi R, Akiyama T, Kato M, et al. Comprehensive targeted next-generation sequencing in Japanese familial amyotrophic lateral sclerosis. Neurobiol Aging. 2017;53:194.e1-.e8.
98. Mitsuzawa S, Akiyama T, Nishiyama A, Suzuki N, Kato M, Warita H, et al. TARDBP p.G376D mutation, found in rapid progressive familial ALS, induces mislocalization of TDP-43. eNeurologicalSci. 2018;11:20-2.
99. Korb MK, Kimonis VE, Mozaffar T. Multisystem proteinopathy: Where myopathy and motor neuron disease converge. Muscle Nerve. 2021;63(4):442-54.
100. Franzmann TM, Alberti S. Prion-like low-complexity sequences: Key regulators of protein solubility and phase behavior. J Biol Chem. 2019;294(18):7128-36.
101. Le Gall L, Duddy WJ, Martinat C, Mariot V, Connolly O, Milla V, et al. Muscle cells of sporadic amyotrophic lateral sclerosis patients secrete neurotoxic vesicles. Journal of Cachexia, Sarcopenia and Muscle. 2022;13(2):1385-402.
102. Gagliardi D, Bresolin N, Comi GP, Corti S. Extracellular vesicles and amyotrophic lateral sclerosis: from misfolded protein vehicles to promising clinical biomarkers. Cellular and Molecular Life Sciences. 2021;78(2):561-72.
103. Mori F, Tada M, Kon T, Miki Y, Tanji K, Kurotaki H, et al. Phosphorylated TDP-43 aggregates in skeletal and cardiac muscle are a marker of myogenic degeneration in amyotrophic lateral sclerosis and various conditions. Acta Neuropathologica Communications. 2019;7(1):165.
104. Lépine S, Castellanos-Montiel MJ, Durcan TM. TDP-43 dysregulation and neuromuscular junction disruption in amyotrophic lateral sclerosis. Translational Neurodegeneration. 2022;11(1):56.
105. Tawara N, Yamashita S, Kawakami K, Kurashige T, Zhang Z, Tasaki M, et al. Muscle-dominant wild-type TDP-43 expression induces myopathological changes featuring tubular aggregates and TDP-43-positive inclusions. Exp Neurol. 2018;309:169-80.
106. Pongrácová E, Buratti E, Romano M. Prion-like Spreading of Disease in TDP-43 Proteinopathies. Brain Sciences. 2024;14(11):1132.
107. Hayes LR, Kalab P. Emerging Therapies and Novel Targets for TDP-43 Proteinopathy in ALS/FTD. Neurotherapeutics. 2022;19(4):1061-84.
108. Becker LA, Huang B, Bieri G, Ma R, Knowles DA, Jafar-Nejad P, et al. Therapeutic reduction of ataxin-2 extends lifespan and reduces pathology in TDP-43 mice. Nature. 2017;544(7650):367-71.
109. Ionis-Pharmaceuticals. Ionis and Biogen Announce Topline Phase 1/2 Study Results of Investigational Drug in Amyotrophic Lateral Sclerosis. News release. 2024 [Available from: https://www.prnewswire.com/news-releases/ionis-and-biogen-announce-topline-phase-12-study-results-of-investigational-drug-in-amyotrophic-lateral-sclerosis-302147377.html.
110. Davydov EV, Goode DL, Sirota M, Cooper GM, Sidow A, Batzoglou S. Identifying a high fraction of the human genome to be under selective constraint using GERP++. PLoS Comput Biol. 2010;6(12):e1001025.
111. Pollard KS, Hubisz MJ, Rosenbloom KR, Siepel A. Detection of nonneutral substitution rates on mammalian phylogenies. Genome Res. 2010;20(1):110-21.
112. Choi Y, Sims GE, Murphy S, Miller JR, Chan AP. Predicting the functional effect of amino acid substitutions and indels. PLoS One. 2012;7(10):e46688.

113. Kumar P, Henikoff S, Ng PC. Predicting the effects of coding non-synonymous variants on protein function using the SIFT algorithm. Nat Protoc. 2009;4(7):1073-81.
114. Adzhubei IA, Schmidt S, Peshkin L, Ramensky VE, Gerasimova A, Bork P, et al. A method and server for predicting damaging missense mutations. Nat Methods. 2010;7(4):248-9.
115. Kircher M, Witten DM, Jain P, O'Roak BJ, Cooper GM, Shendure J. A general framework for estimating the relative pathogenicity of human genetic variants. Nat Genet. 2014;46(3):310-5.
116. Chun S, Fay JC. Identification of deleterious mutations within three human genomes. Genome Res. 2009;19(9):1553-61.
117. Carter H, Douville C, Stenson PD, Cooper DN, Karchin R. Identifying Mendelian disease genes with the variant effect scoring tool. BMC Genomics. 2013;14 Suppl 3(Suppl 3):S3.
118. Niroula A, Vihinen M. How good are pathogenicity predictors in detecting benign variants? PLoS Comput Biol. 2019;15(2):e1006481.
119. Schwarz JM, Rödelsperger C, Schuelke M, Seelow D. MutationTaster evaluates disease-causing potential of sequence alterations. Nat Methods. 2010;7(8):575-6.
120. López-Ferrando V, Gazzo A, de la Cruz X, Orozco M, Gelpí JL. PMut: a web-based tool for the annotation of pathological variants on proteins, 2017 update. Nucleic Acids Res. 2017;45(W1):W222-w8.
121. Jagadeesh KA, Wenger AM, Berger MJ, Guturu H, Stenson PD, Cooper DN, et al. M-CAP eliminates a majority of variants of uncertain significance in clinical exomes at high sensitivity. Nat Genet. 2016;48(12):1581-6.
122. Shihab HA, Gough J, Cooper DN, Stenson PD, Barker GL, Edwards KJ, et al. Predicting the functional, molecular, and phenotypic consequences of amino acid substitutions using hidden Markov models. Hum Mutat. 2013;34(1):57-65.
123. Malhis N, Jacobson M, Jones SJM, Gsponer J. LIST-S2: taxonomy based sorting of deleterious missense mutations across species. Nucleic Acids Res. 2020;48(W1):W154-w61.
124. Raimondi D, Tanyalcin I, Ferté J, Gazzo A, Orlando G, Lenaerts T, et al. DEOGEN2: prediction and interactive visualization of single amino acid variant deleteriousness in human proteins. Nucleic Acids Res. 2017;45(W1):W201-w6.
125. Karczewski KJ, Francioli LC, Tiao G, Cummings BB, Alföldi J, Wang Q, et al. The mutational constraint spectrum quantified from variation in 141,456 humans. Nature. 2020;581(7809):434-43.
126. Fu W, O'Connor TD, Jun G, Kang HM, Abecasis G, Leal SM, et al. Analysis of 6,515 exomes reveals the recent origin of most human protein-coding variants. Nature. 2013;493(7431):216-20.
127. Sudmant PH, Rausch T, Gardner EJ, Handsaker RE, Abyzov A, Huddleston J, et al. An integrated map of structural variation in 2,504 human genomes. Nature. 2015;526(7571):75-81.

# Appendix

**Table 20: Evolutionary conservation of residues affected by *TARDBP* variants** (adapted from (62))

| Conservation score | c.1039T>C (p.Ser347Pro) | c.1127G>T (p.Gly376Val) |
|---|---|---|
| GERP++ score[a)] | 5.81 | 5.81 |
| PhastCons 100way vertebrate[b)] | 1.00 | 1.00 |
| PhyloP 100way vertebrate[b)] | 5.642 | 6.972 |

[a)] GERP++ estimates the evolutionary constraint at specific genomic positions based on alignments across 36 mammalian species. Scores range from -12.36 to 6.18, with higher values indicating stronger conservation during mammalian evolution (110).
[b)] PhastCons and PhyloP are conservation metrics derived from multiple sequence alignments of 100 vertebrate genomes. PhastCons scores range from 0 to 1, while PhyloP scores range from -20 to 9.87. Higher scores of each reflect greater evolutionary conservation at the respective genomic position (111).

**Table 21: Pathogenicity predictions for *TARDBP* variants** (adapted from (62))

| Prediction tool | c.1039T>C (p.Ser347Pro) | c.1127G>T (p.Gly376Val) |
|---|---|---|
| PROVEAN prediction (score)[a)] | neutral (0.51) | damaging (-2.56) |
| SIFT prediction (score)[b)] | tolerated (0.26) | deleterious (0.01) |
| PolyPhen-2 prediction (score)[c)] | possibly damaging (0.593) | benign (0.086) |
| CADD phred-like score[d)] | damaging (22.8) | damaging (23.8) |
| LRT prediction (LRTnew score)[e)] | deleterious (1.00) | deleterious (1.00) |
| VEST prediction score[f)] | harmful (0.577) | harmful (0.795) |
| MutationTaster2 prediction (score)[g)] | disease causing (1.00) | disease causing (1.00) |
| PMut prediction (score)[h)] | neutral (0.17) | neutral (0.42) |
| M-CAP prediction (score)[i)] | damaging (0.077) | damaging (0.040) |
| FATHMM prediction (score)[j)] | damaging (-2.35) | damaging (-2.25) |
| LIST-S2 prediction (score)[k)] | damaging (0.88) | damaging (0.89) |
| DEOGEN2 prediction (score)[l)] | tolerated (0.274) | damaging (0.661) |

[a)] PROVEAN scores ≤-2.50 are considered 'deleterious' (112).
[b)] SIFT scores <0.05 are assigned the prediction 'damaging' (113).
[c)] PolyPhen-2 scores closer to 1 suggest a higher probability of a 'damaging' effect (114).
[d)] CADD Phred-like rank scores >15 (or >20 for a more conservative threshold) are considered indicative of 'damaging' variants (115).
[e)] LRTnew scores range from 0 to 1, with higher values implying an increased likelihood of a variant being 'deleterious' (116).
[f)] VEST scores range from 0 to 1; higher values suggest a greater probability of functional impact (117). A score of 0.5 has been suggested as a cut-off between harmful and benign (118).
[g)] MutationTaster2 reports a probability value reflecting the confidence of its prediction; values close to 1 indicate high certainty (119).
[h)] The PMut classifier assigns scores from 0 to 1: variants scoring 0-0.5 are classified as 'neutral', while those scoring 0.5-1 are predicted as 'disease-causing' (120).

[i] M-CAP scores range from 0 to 1, with higher values reflecting a greater likelihood of being 'damaging'. A score of 0.5 serves as the threshold between 'damaging' and 'tolerated' (121).
[j] FATHMM scores range from -16.13 to 10.64; lower scores are associated with increased likelihood of pathogenicity. The cutoff for 'damaging' is -1.5 (122).
[k] LIST-S2 scores range from 0 to 1, with higher values indicating greater pathogenic potential. A score ≥0.85 is considered 'deleterious' (123).
[l] DEOGEN2 scores range from 0 to 1; higher values suggest a stronger likelihood of pathogenicity. A cutoff of 0.5 separates 'damaging' from 'tolerated' variants (124).

**Table 22: Frequencies of *TARDBP* variants in control data sets** (adapted from (62))

| Data set | Number of samples | c.1039T>C (p.Ser347Pro) | c.1127G>T (p.Gly376Val) |
|---|---|---|---|
| GnomAD[a] | 138,632 | 0 | 0 |
| ESP6500[b] | 6,503 | 0 | 0 |
| 1000G[c] | 2,504 | 0 | 0 |

[a] The Genome Aggregation Database (gnomAD) covers sequencing data from exomes and genomes of unrelated individuals, collected through various disease-specific and population-based genetic studies (125).
[b] The NHLBI GO Exome Sequencing Project (ESP) includes exome data from individuals affected by cardiac, pulmonary, or hematopoietic disorders (126).
[c] The 1000 Genomes Project (1000G) contains whole-genome data from individuals who self-reported as healthy at the time of sample collection (127).

# Publications

## Presentations

**Zibold J**, Wiessner M, Topf A, Petiot P, Stucka R, Dusl M, Krause S, Schoser B, Walter M, Straub V, Urtizberea A, Klopstock T, Senderek J
TDP43 gene variants in patients with autosomal dominant degenerative myopathy (EPR3088).
European Academy of Neurology (EAN) Congress, Norway, 2019 July

**Zibold J**, Wiessner M, Topf A, Petiot P, Stucka R, Dusl M, Krause S, Schoser B, Walter M, Straub V, Urtizberea A, Klopstock T, Senderek J
TDP43-Varianten bei autosomal dominanter distaler Myopathie.
Deutsche Gesellschaft für Muskelkranke (DGM) Congress, Germany, 2019 May

## Publication

**Zibold J**, Lessard LER, Picard F, da Silva LG, Zadorozhna Y, Streichenberger N, Belotti E, Osseni A, Emerit A, Errazuriz-Cerda E, Michel-Calemard L, Menassa R, Coudert L, Wiessner M, Stucka R, Klopstock T, Simonetti F, Hutten S, Nonaka T, Hasegawa M, Strom TM, Bernard E, Ollagnon E, Urtizberea A, Dormann D, Petiot P, Schaeffer L, Senderek J, Leblanc P.
The new missense G376V-TDP-43 variant induces late-onset distal myopathy but not amyotrophic lateral sclerosis.
Brain. 2024 May 3;147(5):1768-1783.

doi: 10.1093/brain/awad410. PMID: 38079474; PMCID: PMC11068115.

# Acknowledgements

Firstly, I would like to thank my supportive supervisor, Prof. Dr. Jan Senderek, who allowed me to conduct this project in his laboratory and has given me constant advice. His immense knowledge and passion for science were always inspiring.

I thank Prof. Dr. Thomas Klopstock for introducing me to the academic research world and for his outstanding guidance during my studies. The joint EAN congress in Oslo was especially a highlight.

Special thanks go to all the members of the Laboratory of Molecular Myology for their supportive cooperation. In particular, I would like to thank Dr. Rolf Stucka for his detailed teaching of experimental approaches. I thank Prof. Dr. Dorothee Dormann and Lara Aletta Gruijs da Silva for the excellent and professional collaboration.

My vast appreciation goes to my parents for all their encouragement and support. Finally, I want to thank Kaj for energizing me and having my back no matter what.

# Affidavit

Zibold, Julia Konstanze

Surname, first name

I hereby declare, that the submitted thesis entitled:

**TARDBP variants cause late-onset distal myopathy**

is my own work. I have only used the sources indicated and have not made unauthorised use of services of a third party. Where the work of others has been quoted or reproduced, the source is always given.

I further declare that the dissertation presented here has not been submitted in the same or similar form to any other institution for the purpose of obtaining an academic degree.

Munich, February 17, 2026

Place, Date

Julia Konstanze Zibold

Signature doctoral candidate